Advanced Nanocomposites 1 (2024) 318–343

Contents lists available at ScienceDirect

Advanced Nanocomposites

journal homepage: www.keaipublishing.com/en/journals/advanced-nanocomposites/

Surface-initiated atom transfer radical polymerization for the preparation and applications of brush-modified inorganic nanoparticles

Yingxue Liu[a], Jiadong Wang[a], Feichen Cui[b], Yang Han[a], Jiajun Yan[b,*], Xuan Qin[a,c,*], Liqun Zhang[a,*], Krzysztof Matyjaszewski[c,d,*]

[a] State Key Laboratory of Organic-Inorganic Composites, Beijing University of Chemical Technology, Beijing 100029, China
[b] School of Physical Science and Technology, ShanghaiTech University, Shanghai 201210, China
[c] Department of Chemistry, Carnegie Mellon University, 4400 Fifth Avenue, Pittsburgh, PA 15213, United States
[d] Department of Molecular Physics, Faculty of Chemistry, Lodz University of Technology, str. Żeromskiego 116, 90924 Łódź, Poland

ARTICLE INFO

Keywords:
Particle brush
Inorganic nanoparticles
Hybrid materials
Surface-initiated atom transfer radical polymerization

ABSTRACT

Surface-Initiated Atom Transfer Radical Polymerization (SI-ATRP) is a pivotal technique in materials science, essential for growing polymer brushes on the surfaces of inorganic nanoparticles to create advanced polymer/inorganic nanocomposites. SI-ATRP originates from the broader ATRP methodology. ATRP involves a reversible redox process mediated by transition metal catalysts, which control radical polymerization. SI-ATRP extends this mechanism to surfaces, allowing for the precise grafting of polymer chains directly from nanoparticle substrates. The core of this technique lies in the careful selection and modification of nanoparticle surfaces to introduce effective ATRP initiators. One of the fundamental systems in this domain is inorganic nanoparticles grafted with polymer brushes, which are characterized by adjustable molecular attributes and intricate interactions. These systems provide a versatile platform for designing and synthesizing novel materials with diverse properties and applications, where particle brushes act as

Abbreviations: APTES, 3-Aminopropyl triethoxysilane; ARGET ATRP, Activators regenerated by electron transfer ATRP; ATRP, Atom transfer radical polymerization; BA, Butyl acrylate; BHE, (6-(2-Bromo-2-methyl)propionyloxyhexyl)triethoxysilane; BHCS, (6-(2-Bromo-2-methyl)propionyloxy)hexyl dimethylchlorosilane; BHTS, (6-(2-Bromo-2-methyl)propionyloxy)hexyl trichlorosilane; BiBADA, 12–(2-Bromoisobutyramide)dodecanoic acid; BIDS, (3-(2-Bromoisobutyryl) oxypropyl)dimethylethoxysilane; BPCS, (3-(2-Bromo-2-methyl) propionyloxy)propyl dimethylchlorosilane; BPDS, (3-(2-Bromopropionyl) oxypropyl) dimethylethoxysilane; BPE, (3-(2-Bromo-2-methyl)propionyloxypropyl)triethoxysilane; BPES, (15-(2-Bromoisobutyryl)oxypentadecyl)dimethylethoxysilane; BPTS, (3-(2-Bromo-2-methyl)propionyloxy)propyl trichlorosilane; BUCS, (11-(2-Bromo-2-methyl)propionyloxy)undecyl dimethylchlorosilane; BUES, (11-(2-Bromoisobutyryl) oxyundecyl)dimethylethoxysilane; BUTS, (11-(2-Bromo-2-methyl)-propionyloxy)undecyl trichlorosilane; CDES, (2-(4-Chloromethylphenyl) ethyl)dimethylethoxysilane; CMPES, ((*p*-Chloromethyl) phenylethyl)-trimethoxysilane; CMPS, ((*p*-Chloromethyl phenyl)trimethoxysilane; CMPTS, 4-(Chloromethyl)phenyl trichlorosilane; CPB, Concentrated polymer brush; CRP, Controlled radical polymerization; CUTS, 11–(2-Chloropropionyloxy)undecyl trichlorosilane; DTZ, Diphenylthiocarbazone; DP_n, Number of average polymerization degree; *e*ATRP, Electrochemically mediated ATRP; EGaIn, Eutectic gallium indium; HAL, Hhermoplasma acidophilum histidine ammonia lyase; 2HEA, 2-Hydroxyethyl acrylate; HBP, Hyperbranched aromatic polyamide; ICAR ATRP, Initiators for continuous activator regeneration ATRP; JP, Janus particles; Mb, Msyoglobin; MBA, *N,N*-methylenebisacrylamide; Mechano/sono ATRP, Mechanically/ultrasound induced ATRP; MIPMSEA, (2-(methacryloyloxy)ethyl methanesulfonate)-based myoglobin molecular-imprinted polymers; MSEA, (2-(methylsulphonyl) ethyl acrylate; MW, Molecular weight; MWD, Molecular weight distribution; NIPAM, *N*-isopropylacrylamide; NMP, Nitroxide-mediate polymerization; O-ATRP, Photoinduced organocatalyzed ATRP; PAA/PAC, Poly(acrylic acid); PBA, Poly(*n*-butyl acrylate); PBMA, Poly(*n*-butyl methacrylate); PBS, Phosphate buffer saline; PDEA, Poly (methacrylic acid (2-(diethylamino)ethyl ester)); PDEAEMA, Poly(2-(*N,N*-diethylamino)-ethyl methacrylate)); PDMAEMA, Poly(*N, N*-dimethylaminoethyl methacrylate); PEG, Polyethylene glycol; Photo-ATRP, Photo-induced ATRP; PMMA, Polymethyl methacrylate; PMBTMA, Poly(2-mercaptobenzothiazole); PNIPAM, Poly (*N*-isopropylacrylamide); PNVCL, Poly(*N*-vinylcaprolactam); POEGMA, Poly(oligo(ethylene glycol) methyl ether methacrylate); PI, Polyisoprene; PIL, Poly (ionic liquid); PSt, Polystyrene; PSPMA, Poly(3-sulfopropyl methacrylate potassium); P*t*BA, Poly(*tert*-butyl acrylate); RAFT, Reversible addition–fragmentation chain transfer polymerization; ROMP, Ring-opening metathesis polymerization; SARA-ATRP, Supplemental activators and reducing agents ATRP; SDPB, Semidilute particle brush; SEC, Size exclusion chromatography; SEM, Scanning electron microscopy; SI-ATRP, Surface-initiated atom transfer radical polymerization; SCVP, Self-coagulating vinyl polymerization; TEM, Transmission electron microscopy; TGA, Thermogravimetic analysis; uSI-ATRP, Ultrasound-mediated SI-ATRP; WSD, Wear scar diameter; 2-BiB, 2-Bromoisobutyryl bromide; 4VP, 4-Vinylpyridine

Peer review under responsibility of KeAi Communications Co., Ltd.

* Corresponding authors.
E-mail addresses: yanjj@shanghaitech.edu.cn (J. Yan), qinxuan@mail.buct.edu.cn (X. Qin), zhanglq@mail.buct.edu.cn (L. Zhang), km3b@andrew.cmu.edu (K. Matyjaszewski).

https://doi.org/10.1016/j.adna.2024.09.002
Received 11 July 2024; Received in revised form 13 September 2024; Accepted 28 September 2024
Available online 5 October 2024

one-component composite materials or multifunctional fillers for high-performance nanocomposites. They are driving innovation in nanotechnology, biotechnology and materials engineering. This review critically examines the molecular design of tethered polymer chains from various particles and the development of particle brush materials for applications in energy, medical and catalytic fields, as well as in advanced nanocomposites with enhanced mechanical properties, responsiveness, optical properties, dielectric properties and transmission characteristics.

1. Introduction

Surface-initiated atom transfer radical polymerization (SI-ATRP) represents a significant advancement in the field of macromolecular science, particularly in the context of creating well-defined polymer structures on inorganic nanoparticles. This technique stems from the broad category of atom transfer radical polymerization (ATRP), which has revolutionized the way polymers are synthesized, by offering precise design over molecular weights and polymer architectures.

The origins of ATRP, established in the mid-1990s, marked a pivotal shift from traditional free radical polymerization techniques that suffered from limitations, such as uncontrollable molecular weight distributions and lack of functionality in the resulting polymers [1,2]. ATRP addresses these challenges by utilizing a transition metal catalyst to mediate the polymerization process, allowing for reversible activation and deactivation of the polymer chain ends [3]. This mechanism not only enables a more uniform polymer growth but also facilitates the synthesis of block copolymers, gradient copolymers and polymers with complex architectures [4,5].

Building upon the robust framework of ATRP, SI-ATRP extends its capabilities directly to surfaces [6]. This adaptation involves anchoring an ATRP initiator to the surface of materials, such as inorganic nanoparticles, thereby localizing the polymerization process at the surface. The rationale behind this technique is to harness the inherent properties of ATRP while integrating polymers to substrates that could benefit from polymer-based functionalization. Inorganic nanoparticles, widely recognized for their unique optical, electrical and magnetic properties, are thus prime candidates for SI-ATRP due to the potential for significantly enhancing their functionality.

The application of SI-ATRP to inorganic nanoparticles begins with the careful selection and modification of the nanoparticle surface to introduce ATRP initiators. This process is crucial as it dictates the density and activity of the initiating sites, which in turn influence the growth kinetics and structure of the polymer chains. Once the initiators are in place, the polymerization can be conducted under controlled conditions to graft polymers directly from the nanoparticle surface. This method effectively creates a hybrid material that combines the intrinsic properties of the nanoparticles with the versatility of polymers.

The structural control offered by SI-ATRP is particularly beneficial for tailoring the interfacial interactions between the nanoparticles and their environments. By adjusting the length, density and composition of the grafted polymer chains, it is possible to influence properties such as solubility, stability and reactivity. These modifications can be designed to promote dispersion in solvents, compatibility with polymer matrices, or targeted interaction with biological molecules, opening up applications in drug delivery, catalysis and electronic devices.

Moreover, SI-ATRP is not just limited to enhancing the properties of inorganic nanoparticles but also provides a platform for the creation of advanced composite materials. Through the strategic design of polymer brushes, nanoparticles can be assembled into ordered structures or embedded within larger polymer matrices to yield materials with novel properties. Such composites are of great interest for creating high-performance materials that leverage the synergistic benefits of both polymers and inorganic nanoparticles.

Therefore, SI-ATRP stands as a transformative technique in materials science, enabling the precise and efficient modification of inorganic nanoparticles with polymers. As research in this field continues to evolve, it is anticipated that SI-ATRP will find increasing applications across a broad spectrum of technologies, driving innovations in nanotechnology, biotechnology and materials engineering [7,8]. The next sections will delve deeper into specific aspects of inorganic nanoparticle modification, the structural regulation of polymer chains and the diverse applications that benefit from this advanced polymerization technology.

2. Preparation of brush-modified nanoparticles *via* SI-ATRP

2.1. SI-ATRP overview

Since first reported in 1995 [9], ATRP has been gradually developed into the most effective and robust controlled radical polymerization(CRP) technique due to its ability to prepare precisely defined polymers with well-controlled polymerization kinetics under mild conditions [2]. It has also become the primary method for the preparation of polymers/inorganic hybrid particles via surface-initiated polymerization [10,11]. In conventional ATRP, the active center is generated by a reversible redox process of a transition metal complex (X–Mt^m/L), where Mt^m is usually Cu^I, X represents a (pseudo)halogen, and L is the ligand. For the sake of clarity, the counterion is omitted from this description. In this process, the metal is oxidized and simultaneously, a halogen atom is abstracted from the dormant species (an alkyl halide, P_n–X) to obtain active radicals (propagating radical or active species, P_n·). Consequently, a metal halide complex in a higher oxidation state, X–Mt^{m+1}, is formed. The mechanism of ATRP is depicted in Fig. 1. This procedure has a rate constant of k_{act}. A propagating chain behaves in a manner similar to that of the conventional free radical polymerization, *i.e.*, either adding to a monomer (with a rate constant of k_p) or terminating with another radical by coupling or disproportionation (with a rate constant of k_t). In an ATRP process specifically, however, it may also undergo a fast-reversible deactivation *via* the aforementioned redox equilibrium (with a rate constant k_{deact}) to form halide-terminated dormant polymer chains [4,12].

In well-controlled ATRP reactions, less than a few percent of polymer chains undergo termination due to the persistent radical effect and $k_{act} < < k_{deact}$. In ATRP, due to fast initiation and rapid reversible deactivation, the terminal radicals on any single chain are only active for a short period of time, and a restricted quantity of monomer is introduced to the propagating radicals during each period of activity. Consequently, all polymer chains concurrently grow at a uniform rate, facilitating the attainment of polymers with well-controlled molar masses and narrow molecular weight distributions [11]. The kinetics and control in ATRP are influenced by the concentrations of both the deactivator (X–Mt^{m+1}/L) and the activator (Mt^m/L), according to Eq.

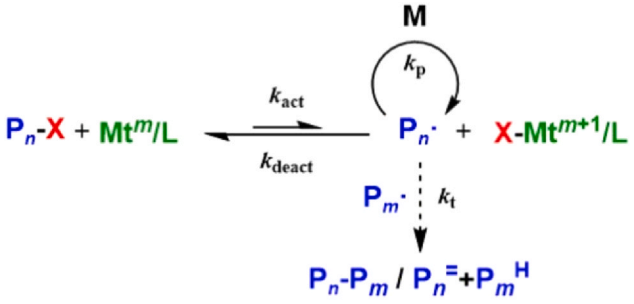

Fig. 1. Illustration of the ATRP equilibrium.

(1). R_p depends on the propagating rate constant k_p, the ratio of the activation rate constant k_{act} to the deactivation rate constant k_{deact}, which is the ATRP equilibrium constant $K_{ATRP} = k_{act}/k_{deact}$ predominantly determined by the structures of the ligand and the halide chain end. The polymer number average degree of polymerization (DP_n) is determined by the ratio of monomer concentration consumed to the initial initiator concentration ($\Delta[M]/[RX]_0$) and monomer conversion, independent of transition metal concentration. The higher the monomer conversion rate, the higher the deactivator concentration, and the lower the dispersity.

$$R_p = -\frac{d[M]}{dt} = k_p[M][RX] = k_p[M]K_{ATRP}[RX]([Mt^m/L]/[[X - Mt^{m+1}/L] \quad (1)$$

$$\frac{M_w}{M_n} = 1 + \frac{1}{DP_n} + \left(\frac{[RX]_0 k_p}{k_{deact}[X - Mt^{m+1}/L]}\right)\left(\frac{2}{Conv.} - 1\right) \quad (2)$$

In this review, we discuss chains grown *in-situ* from hard functionalized inorganic surfaces by "grafting-from" (*vide infra*), and the mechanism of SI-ATRP growth is different from that of the conventional ATRP based on untethered initiator initiation. Firstly, initiation sites are anchored to the surface *via* coupling techniques prior to polymerization. Secondly, monomers need to diffuse to the particle surface during polymer growth, potentially limiting chain growth rates and thereby influencing polymerization kinetics [13].

If the deactivator concentration is low, reversible deactivation will not take place, leading to the prevalence of irreversible radical termination. As predicted by Flory's theory of gelation, in the case of interparticle termination, only 0.1 % termination is needed to generate macroscopic gels of nanoparticles with thousands of tethered chains in SI-ATRP [14]. Microemulsion polymerization can reduce gelation and enable the preparation of particle brushes with high conversion rates and high grafting densities [15].

In order to better control molecular weight and molecular weight distribution, a sufficient amount of deactivator is required in the system, as depicted in Eq. (2) [16]. Furthermore, since each act of termination consumes the same amount of activator, traditional ATRP is conducted in relatively high catalyst concentrations to counteract the unavoidable free radical terminations and interference from oxygen. The catalyst concentration typically ranges from 0.1 to 1 mol/L with strict anaerobic conditions required during the polymerization [17]. The use of transition metals in ATRP poses environmental concerns and increases the cost of product purification, thereby constraining applications [18]. In contrast, modern ATRP techniques, which rely on the continuous regeneration of catalysts in response to various external stimuli, permit catalyst utilization at ppm levels and offer oxygen tolerance [5,19–22]. These techniques include (i) activators regenerated by electron transfer (ARGET) ATRP [23,24] with common reducing agents including stannous octoate [25], ascorbic acid [26], sulfites and amines, (ii) initiators for continuous activator regeneration (ICAR) ATRP [27], (iii) zerovalent metals as the supplemental activators and the reducing agents (SARA) ATRP [28], (iv) electrochemically mediated ATRP (*e*ATRP) [29–31], (v) photochemically-mediated ATRP (photo-ATRP) [32,33], (vi) mechanically/ultrasound induced ATRP (mechano/sono-ATRP) [34–38] and (vii) metal-free ATRP/organocatalyzed ATRP (O-ATRP) [32,39,40].

Controlled radical polymerization (CRP) is the most suitable method for polymer grafted from nanoparticle surfaces; among various CRP techniques, SI-ATRP offers several advantages. These include simple experimental setup and availability of cost-effective and readily accessible catalysts that can form complexes with commercially available or easily synthesized ligands such as alkylamines, imines or pyridine derivatives. SI-ATRP also utilizes commercially available or easily prepared alkyl halides as initiators or macroinitiators prepared through the surface modification of solid substrates. Additionally, compared to reversible addition–fragmentation chain transfer (RAFT) polymerization with tethered chain transfer agents and nitroxide-mediated polymerization (NMP), SI-ATRP allows for much higher concentrations of deactivator relative to active chains, enhancing the control over polymerization from surfaces. Furthermore, mechanistically, unlike surface RAFT, typical SI-ATRP systems do not produce untethered radical species that lead to free polymer as an impurity in the bulk solution. Anionic and cationic polymerizations require monomers with specific electronic properties and must be conducted under strict anhydrous and oxygen-free conditions. Ring-Opening Metathesis Polymerization (ROMP) is primarily suitable for cyclic olefin monomers and typically requires specific catalysts, which are often expensive. In contrast, ATRP offers significant advantages over anionic/cationic polymerization and ROMP in terms of monomer versatility, operational conditions and process economics.

2.2. Surface functionalization of inorganic nanoparticles

The choice of inorganic surfaces for SI-ATRP depends on the intended application. Recently, core/shell nano-hybrids, comprising a nanoparticle core and a polymer brush shell, have attracted significant interest in research fields such as nanoelectronics, nanophotonics, catalysis, nanopatterning, drug delivery and biosensing. This review focuses on *in-situ* polymerization via SI-ATRP from nanostructured inorganic particle surfaces. Various substrates, such as silica, graphite, alumina, titania, iron oxide, gold, quantum dots and other organic and biological materials, have been used to meet different requirements. Fig. 2 presents an illustration of the grafting of ATRP-active Cl or Br groups onto the surface of typical inorganic nanoparticles. The "grafting-from" method involves attaching a polymerization initiator to the particle surface, allowing controlled polymer growth and achieving higher density and uniformity. This technique is particularly useful for complex substrates and supports a wide range of monomers. The synthesis of hybrid particles with silica, metals, metal oxides and carbon materials as cores is classified and discussed.

2.2.1. Silica

Due to its high rigidity, thermal stability and physical and chemical resistance, silica has been extensively studied and applied in various fields such as colloid chemistry, catalysis, nanopatterning, photonics, drug delivery and biosensing [41]. Owing to their widespread applications and surfaces covered with readily modifiable Si-OH groups, silica nanoparticles are the most commonly used inorganic substrate of hybrid particles prepared *via* SI-ATRP. These hybrid materials integrate rigidity and stability of silica nanoparticles with the flexibility, processability and functionality of organic polymers, broadening the potential applications of silica nanoparticles. ATRP initiators can be covalently bonded to the surface of silica nanoparticles [42] by 1) attaching pre-synthesized functional silane containing an initiator moiety and an alkoxy/halosilane group capable of coupling with a silica surface on each end, or 2) by employing commercially available functional

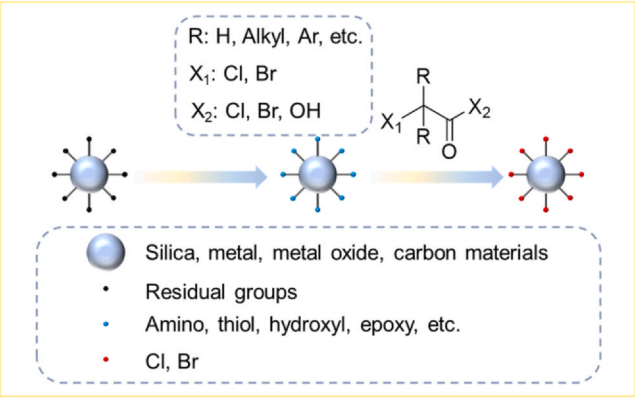

Fig. 2. Surface functionalization of inorganic nanoparticles.

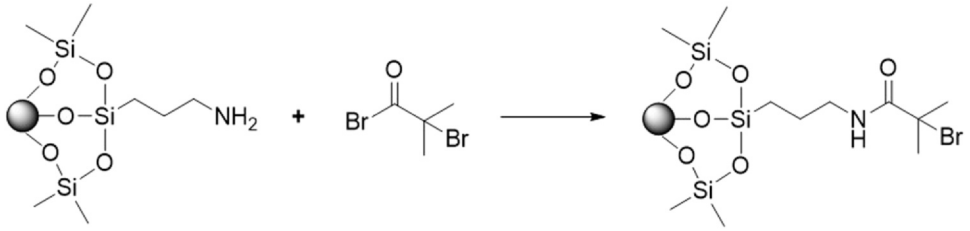

Fig. 3. The reaction between APTES modified nanoparticles and the commonly used ATRP initiator precursor 2-BiB.

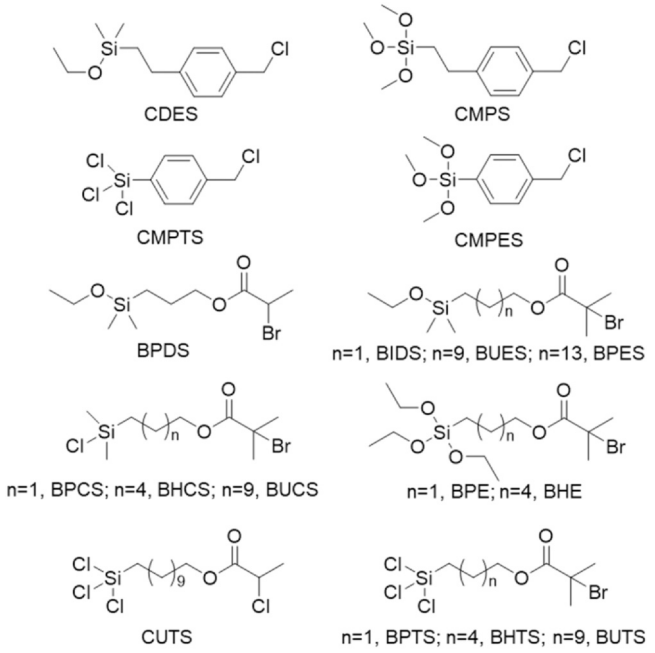

Fig. 4. Functional initiators used for SI-ATRP from silica nanoparticles [41].

silane coupling agents to convert surface silanol into amino, thiol, hydroxyl, epoxy groups, etc., ready to react with an acyl halide. Many common functional silane coupling agents, such as 3-aminopropyltriethoxysilane (APTES) and 3-glycidoxypropyltrimethoxysilane, can be obtained from the silicone industry at relatively low prices. The reaction between APTES-modified nanoparticles and the commonly used ATRP initiator precursor α-bromoisobutyryl bromide (2-BiB) is depicted in Fig. 3. Other functional initiators used for SI-ATRP from silica nanoparticles are depicted in Fig. 4.

Silane modification of silica involves one or multiple steps of the reaction, where the structure of the organosilane, particularly the number of hydrolyzable groups, affects the quality of the resulting organosilane layer. Organosilanes containing three polymerizable functional groups exhibit more stable tethering but tend to form multilayer structures. SI-ATRP can graft various polymer ligands from silica surfaces, including polystyrene (PSt), poly(methyl methacrylate) (PMMA), poly(*n*-butyl acrylate) (PBA), poly(*tert*-butyl acrylate) (P*t*BA), poly(methoxy-oligo(ethylene glycol) methacrylate), poly(2-(*n*-morpholine)-ethyl methacrylate), poly(2-hydroxyethyl methacrylate), poly(glyceryl methacrylate), poly(2-(*N*,*N*-dimethylamino)ethyl methacrylate) (PDMAEMA), poly(2-(*N*,*N*-diethylamino)-ethyl methacrylate) (PDEAEMA), as well as polyelectrolytes. Recent reports also demonstrate successful grafting of polyisoprene from the surface of nano-sized silica [43,44]. Thus, the applicability of monomers is diverse and extensive in this context.

2.2.2. Metals

Noble metal nanoparticles (such as Au, Ag, Pt, Pd.) with dimensions smaller than 100 nm exhibit distinctive optical, electrical, catalytic and chemical properties due to surface effects, quantum size effects and

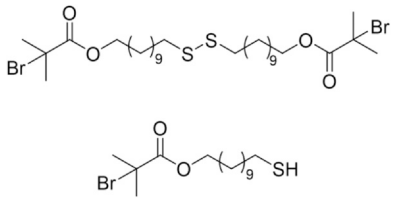

Fig. 5. Structural formula of disulfanediylbis(undecane-11,1-diyl) bis(2-bromo-2-methylpropanoate) and 11-mercaptoundecyl 2-bromo-2-methylpropanoate.

macroscopic quantum tunneling effects. These properties have garnered significant interest across various fields including nanoelectronics, nanophotonics, nanosensors, catalysis and biomedicine [45]. Metals such as Au, Ag, Hg, Fe and Cu can form strong chemical bonds with organic sulfur compounds. By reacting with functional thiols or thiol-terminated polymer chains, disulfides or thiols can be directly grafted onto metal surfaces. As for SI-ATRP, a long alkyl spacer group separates the initiator group of ATRP and the thiol or disulfide group in most cases. The most common disulfides and thiols-based ATRP initiators are disulfanediylbis(undecane-11,1-diyl) bis(2-bromo-2-methylpropanoate) and 11-mercaptoundecyl 2-bromo-2-methylpropanoate, respectively (Fig. 5). Alternatively, hydroxyl-functionalized disulfides or thiols form self-assembled monolayers on metal surfaces, followed by esterification to introduce ATRP initiating moieties. Kitayama et al. [46] modified Au nanoparticles with bis[2-(2-bromoisobutyryloxy)undecyl]disulfide, followed by surface-initiated AGET ATRP of 2-(diethylamino)-ethyl methacrylate. They explored the reversible stabilization-controllability of the hybrid particles in N_2/CO_2 bubbling treatment. The stability of the particles in CO_2 bubbling water increases with the PDEAEMA chain length, as the hybrid particles are stabilized by electrostatic repulsion in CO_2 bubbling water. The stabilizing properties of PDEAEMA-*g*-Au under CO_2/N_2 stimulation may provide ideas for the preparation of reusable nanosensors. Cheng et al. [47] utilized methoxy-poly(ethylene glycol)-thiol to anchor polyethylene glycol (PEG) brushes onto the surface of gold nanoparticles, followed by SI-ATRP to create PEG/PMMA or PEG/PDEAEMA amphiphilic polymer brushes, which is shown in Fig. 6. The resulting hybrid materials self-assembled into two-dimensional arrays at an oil-water interface and the conformation of polymer brushes were modulated in response to stimuli.

2.2.3. Metallic oxide MO_x

There are various types of metal oxides, and to date, there have been numerous reports on the preparation of hybrid particles using aluminum oxide [48], titanium oxide [49], or iron oxide [50] as nanoparticle cores. Research on grafting polymer brushes from the surfaces of other metal oxides such as indium tin oxide [51], zinc oxide [52], copper oxide, nickel oxide and magnesium oxide [53] are gradually expanding.

There are several strategies for modifying metal oxide surfaces. One approach involves the direct reaction between the surface hydroxyl groups (–OH) of metal oxides and acyl halides such as 2-BiB or acryloyl chloride to introduce ATRP-initiating moieties. However, this method often provides limited surface functionality, leading to the aggregation of hybrid materials within the system.

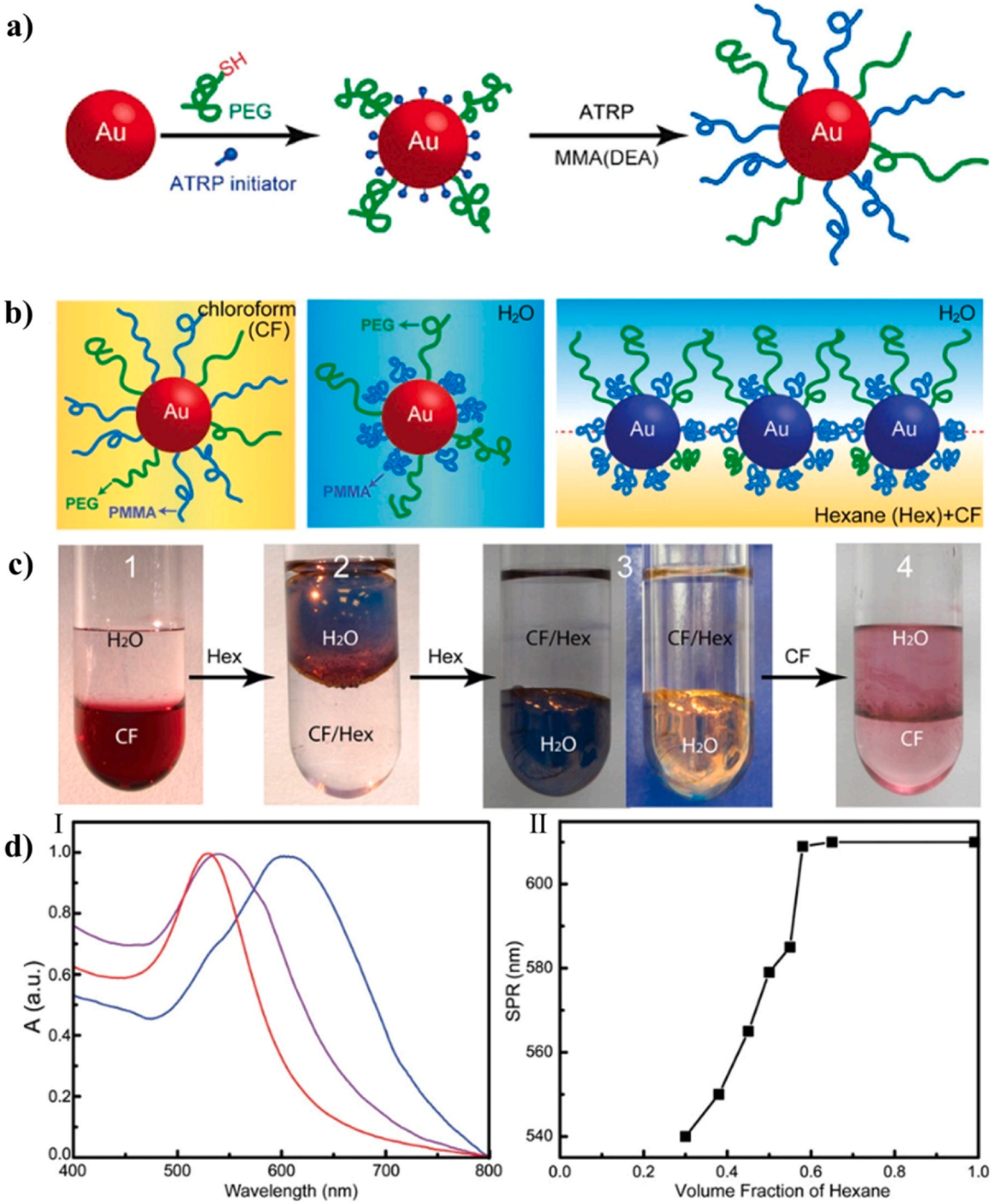

Fig. 6. a) Schematic illustration of the synthesis of amphiphilic gold nanocrystals in the sequentially combined "grafting-to" (co-adsorption PEG and ATRP initiator) and "grafting-from" (SI-ATRP) approaches. b) Schemes of the nanocrystal in chloroform and water and at interfaces. c) Photographs of the assembling process: image 1 shows the mixture of 1.5 mL of H_2O and 1.5 mL of gold nanocrystals chloroform solution; image 2 shows the assembly upon addition of hexane (40 % volume fraction of the organic phase); image 3 shows the assembly when hexane volume fraction is 80 %; and image 4 captures the moment of replacing the hexane–-chloroform mixture with pure chloroform, which shows the dissolution of the assembly upon addition of chloroform. d) (I) UV–vis spectra of the nanocrystal in chloroform (red line), at the interface of water and hexane–chloroform mixtures (purple line, 30 % hexane; blue line, 80 % hexane). (II) Dependence of SPR peaks on the volume fraction of hexane in the oil phase. Reproduced with permission from Ref. [47]. Copyright 2010 American Chemical Society.

Another approach is similar to the surface modification of silica, where low molecular weight organic groups capable of initiating ATRP reactions are tethered onto metal oxide surfaces through either a pre-synthesis or a two-step method. Presynthesized coupling agents used for surface modification are typically bifunctional and synthesized through a series of reactions involving ATRP initiator-precursors, silanes and other compounds. Specifically, one functional group can bind to the nanoparticle surface while the other can initiate the polymerization. For instance, (2-bromo-2-methyl)propanoyloxyhexyltriethoxysilane, synthesized *via* multi-step reactions involving 2-BiB, 5-hexen-1-ol and triethoxysilane, can be grafted onto substrates such as silica [54] or alumina [39]. Otherwise, the condensation reaction of 3-hydroxypropionic acid with 2-BiB is followed by a reaction with the surface hydroxyl groups of ZnO [55]. The two-step method typically involves

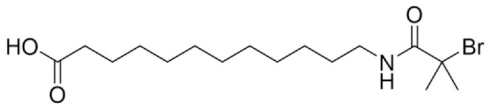

Fig. 7. Structural formula of BiBADA.

secondary modification using 2-BiB to introduce amino, hydroxyl, thiol or carboxyl groups introduced by organic silanes. For instance, the amine functionalization of metallic oxide through reaction with APTES followed by reaction with 2-BiB to yield Fe_3O_4–Br [56], TiO_2–Br, ZrO_2–Br and Al_2O_3–Br [57]. Joh et al. [58] first functionalized the surface-deposited hafnium dioxide on carbon nanotubes using 3-aminopropyltriethoxysilane, followed by secondary modification with 2-BiB to graft poly(oligo(ethylene glycol) methyl ether methacrylate) (POEGMA). This process enabled the research team to fabricate the highest antibody-sensitive carbon nanotube electrochemical biosensor to date. Carboxylates/carboxylic acids can modify the surface of certain metal oxides. Oleic acid, for example, is one of the most commonly used ligands for stabilizing metal and metal oxide nanoparticles. 12-(2-bromoisobutyramido) dodecanoic acid (BiBADA, Fig. 7) is synthesized from ω-aminododecanoic acid, a key building block of Nylon-12. This compound has been demonstrated as an effective universal strategy for the large-scale surface modification of metal oxide nanoparticles. The versatility of BiBADA enables its application across a wide range of nanoparticle systems, making it a significant tool in nanomaterial functionalization [53,59,60].

Compared to carboxylates, phosphates/phosphonic acids form stronger chemical bonds with metal oxide surfaces. However, the supply of organic phosphate/phosphonic acid precursors is strictly regulated by the Chemical Weapons Convention (Annex on Chemicals, Schedule 2). In addition to phosphates, phosphine oxides have been shown to be suitable for anchoring onto certain quantum dots [61]. Apart from silane coupling agents, dopamine and polydopamine, as well as aliphatic amino acids, have gained increasing attention in the field of surface modification chemistry in recent years [62]. Catechol possesses a pentagonal chelating structure that enables the formation of stable adhesion to metal oxide surfaces. Polydopamine, characterized by its high amine and catechol content, is applicable to various irregularly shaped nanoparticles [63]. Additionally, the polydopamine coating can undergo further reactions with other reagents (such as thiols and amine functionalities) through secondary reactions. Yan et al. [64] utilized ultrasonication to induce the formation of an oxide layer on the surface of the liquid metal eutectic gallium indium (EGaIn). Subsequently, BiBADA was assembled on the oxide surface, followed by SI-ATRP grafting of PMMA and poly(*n*-butyl methacrylate) (PBMA) to prepare a series of EGaIn-polymer hybrid materials. Apparent suppression of solidification was observed in these EGaIn nanodroplets stabilized by polymer brushes.

2.2.4. Carbon materials

Carbon materials, including carbon nanotubes, carbon black particles, diamond and graphite, have been employed as the substrates for SI-CRP. Since carbon nanotubes do not possess any functional groups conducive to chemical modification, surface chemical modification is required. For instance, Kong et al. [65] grafted ATRP initiators onto the surface of carbon nanotubes through a multi-step process. Carboxylic acid groups introduced onto the surface of carbon nanotubes by HNO_3 were sequentially reacted with thionyl chloride and ethylene glycol to introduce hydroxyl groups. Building upon the aforementioned method, Jiang et al. [66] further grafted P(BA-*co*-MMA) from the surface, enhancing the dispersibility and mechanical properties of carbon nanotubes in thermoplastic elastomers. Xu et al. [67] developed a high-performance nano-catalyst by attaching gold nanoparticles to the surface of carbon nanotubes. The carbon nanotubes were first functionalized through sequential carboxylic acid functionalization, acylation and hydroxylation. Subsequently, 2-BiB was used for modification on the surface of carbon nanotubes to polymerize 4-vinylpyridine (4VP) *via* ATRP. The resulting product was centrifuged with gold nanoparticles to obtain the final product. This strategy provides an attractive method for the synthesis of CNT-*g*-P4VP/metallic nanoparticle hybrids with promising applications in catalysis.

3. Controlling the architecture of grafted polymers *via* SI-ATRP

The parameters to be controlled in the synthesis of hybrid particles include the molecular weight and its distribution, chemical compositions, grafting density, topological structure and functionality of the grafted chains. This also encompasses various copolymers and brushes with bimodal chain distributions, allowing for the formation of Janus particles [68].

Molecular weight is one of the most critical parameters of a polymer, largely determining its physical properties. With the "livingness" of SI-ATRP, lower molecular weights can be achieved by quenching the reaction at low conversions. On the other hand, high pressures significantly increase the ratio of k_p/k_t, enabling the preparation of PMMA and PSt with molecular weights of approximately 10^6 at room temperature under 6 kbar pressure [69]. Similarly, high molecular weight polymer brushes can be prepared using reverse ATRP in heterogeneous emulsion polymerization [70]. For polymer-grafted nanoparticles, longer grafted chain lengths typically result in more frequent entanglements with surrounding polymer chains, thereby exhibiting higher mechanical strength. Wang et al. [71] grafted PMMA and PSt particle brushes from nano-silica surfaces with varying surface initiating site densities and synthesized ultra-high molecular weight ($M_w > 10^6$) SiO_2-*g*-PMMA particle brushes with narrow molecular weight distributions (< 1.3) and varying grafting densities. Due to the presence of thermal self-initiation reactions in styrene, MMA monomer is more conducive than styrenic monomers for the precise synthesis of ultra-high molecular weight polymer brushes [72].

Controlling the molecular weight distribution (MWD) is more challenging [73]. According to the Eq. (2), MWD is related to the corresponding rate constants, the target degree of polymerization ($[M]_0/[R–X]_0$), conversion and [X–Cu^{II}L]. Adjustment of [X–Cu^{II}L] by varying the total amount of the copper catalyst in the system or fine-tuning K_{ATRP} values by selecting ligands with different activities can be employed to adjust the MWD of grafted chains and achieve a narrower MWD. However, the methods for broadening MWD through controlled polymerization are constrained. For any metal-catalyzed ATRP with catalyst doses in the ppm range, MWD of the product is determined by the concentration of Cu^{II} species. Broadening the MWD of the product can be achieved by reducing the concentration of copper commonly used as a metal catalyst in polymerization [74]. Consequently, this approach enables the preparation of homopolymers and block copolymers with novel morphologies and properties [75]. As the catalyst concentration decreases, the grafting density significantly decreases [76]. Effective control of the MWD can regulate the microstructure of hybrid particles. An appropriately controlled MWD plays a crucial role in the development of stable bicontinuous microstructures. These microstructures have significant potential for applications across various fields, including membranes, biomedicine and conductive polymers. Furthermore, a well-designed MWD enhances the processability of materials, contributing to their broader applicability in advanced technologies.

In addition to molecular weight, high grafting density also ensures that polymer-grafted nanoparticles possess desirable performances [77]. Theoretically, higher grafting densities provide denser polymer interfaces. Grafting density refers to the number of polymer chains per unit area, and it is measured using techniques such as thermal gravimetric analysis (TGA) and size exclusion chromatography (SEC):

$$\sigma = \frac{(1 - f_{NP})N_A \rho_{NP} d}{6 f_{NP} M_n} \quad (3)$$

where, f_{NP} is the mass fraction of inorganic particles determined by TGA; N_A is Avogadro's constant; ρ_{NP} and d are the bulk density and average diameter of the nanoparticles, respectively; and M_n is the number-averaged molecular weight of the polymer brushes determined by SEC.

The grafting density can be tuned by the density of surface-tethered initiating sites, which can be easily adjusted by "dummy" initiators [78,79]. These molecules do not participate in the polymerization reaction but occupy the surface initiation sites, thereby reducing the number of active sites available for the actual polymerization, resulting in a decreased number of polymer chains on the particle brush surface. Moreover, grafting density can also be tuned by the concentration of the Cu catalyst. Yan et al. [74] investigated the effect of varying the initial concentration of the catalyst $[Cu^{II}L]_0$ on the grafting density and dispersity of SiO_2-*g*-PMMA particle brushes synthesized via ARGET ATRP. They found that at high catalyst concentrations (25–200 ppm), the grafting density remained relatively stable. However, at concentrations below 10 ppm, the grafting density significantly decreased as the initial catalyst concentration was reduced. This indicates that there is a critical concentration of the catalyst that regulates grafting density and the type of polymerization. Distinct types of polymerization control were observed above and below this critical concentration. Due to the limited initiation efficiency, the grafting density of the particle brushes decreases as the target molecular weight increases [80].

The grafting density affects the conformation of the grafted chains, forming a mushroom-like shape on the surface of the particles when the grafting density is low. When the grafting density is high, grafted chains in the "concentrated polymer brush" (CPB) regime, which are in close proximity to the particle surface, tend to stretch. However, beyond a critical radius determined by the grafting density, these grafted chains transition into the "semidilute polymer brush" (SDPB) regime, where they adopt a curled conformation. This transition in chain conformation is directly influenced by the grafting density, leading to distinct structural characteristics at different distances from the particle surface [81].

In grafted random copolymer brushes, the arrangement of monomers on the chain is determined by the reactivity ratios of the monomers and their relative concentration in the polymeric medium. Patton et al. [82,83] determined the reactivity ratios for a range of monomers (including styrene, methyl methacrylate, methyl acrylate and 2-vinylpyridine) in surface-initiated copolymerization. Preparing random copolymers requires less control over chain end functionalities, with greater importance placed on monomer feed ratios and copolymerization reactivity ratios. As for well-controlled block copolymer brushes synthesized *via* SI-ATRP, maintaining end-group fidelity is essential. High end-group fidelity and good temporal control can improve the control over the length of block copolymers and aid in designing material properties [29]. Bruening and Baker demonstrated this process in an early study. They showed that after synthesizing each block, using a large excess of $Cu^{II}Br_2$ could retain more than 95 % of active chain ends. In contrast, a simple solvent rinsing technique could retain approximately 85–90 % of active chain ends [84].

The control of the topology of tethered chains is also an important objective in the preparation of hybrid particles. Particle brushes exhibit various topological structures, including cyclic [85], loop-type [86,87] and (hyper)branched. Early reports on polymer loops were often serendipitously observed during the grafting of multi-acid polymer ligands or surface monomer grafting. To date, since the synthesis of cyclic polymer brushes has been exclusively achieved by grafting of pre-synthesized cyclic polymers containing an anchoring unit onto a surface, it is not discussed here. A comprehensive review discusses the preparation, properties and applications of surface-bound polymer loops [88]. The loop-type polymers are commonly prepared *via* a grafting-onto approach using telechelic polymers. Additionally, loop-type brushes can also be synthesized through the post-polymerization modification of linear polymer brushes.

Klok and colleagues [89] converted the free chain ends of linear PMMA brushes to allyl groups, enabling loop closure *via* an olefin metathesis reaction (Fig. 8a,b). (Hyper)branched polymers (Fig. 8c) are synthesized stepwise from solid surfaces using a methodology similar to dendrimer synthesis, or more efficiently through surface-initiated self-condensing vinyl polymerization (SI-SCVP) with inimers such as 4-vinylbenzyl chloride. Each inimer used in SI-SCVP bears both a propagating vinyl moiety and an initiating halide unit. Thus, each step of propagation yields a new branch. Depending on the number of generations of the grafting chains, the simplest branched polymer brushes are bottlebrush polymers with grafts [90,91]. To graft molecular bottlebrushes from a surface, the backbone is typically polymerized from the surface first, followed by the growth of side chains (also termed "grafting-from"). In other cases, macromonomers may be polymerized directly from a surface (termed "grafting-through").

Gradient polymer brushes encompass chemical gradients, molecular weight gradient and grafting density gradients, including variations in composition along the polymer chains. Other more complex gradient forms are often combinations of these four types [92]. Molecular weight gradients can be achieved by gradually changing catalyst concentrations or external stimulus intensity [93]. Grafting density gradients can be achieved by adjusting the initiator density on the surface. ATRP, based on different monomer reactivities or through continuous control of monomer feed, is an effective tool for preparing gradient copolymers *in-situ* [94].

Wang et al. [95] prepared SiO_2-*g*-PBA-*grad*-PMMA particle brushes by slowly adding MMA into a solution of *n*-butyl acrylate (BA) during ARGET ATRP. Improvements in mechanical properties (strength and stiffness) were observed. Because the reactivity ratios of MMA to BA are very different (r_{MMA} = 1.79 and r_{BA} = 0.30), the copolymer system will spontaneously generate gradient copolymer sequence structure. Compared to the alternating and statistical copolymer architectures, the gradient P(MMA/BA) demonstrated superior mechanical performance attributed to the segments segregation to form PMMA-rich cluster regions [96]. Yin et al. [97] polymerized MMA and BA monomers in a one-pot miniemulsion. The compositions and properties of SiO_2-*g*-PMMA-*grad*-PBA particle brushes prepared with five different initial PMMA/PBA molar ratios were compared. The use of heterogeneous reaction medium effectively inhibited the coupling between particle brushes, and the samples showed both high stiffness and toughness when the MMA/BA feeding ratio was 60:40. Schematic illustration of composition-orientation induced mechanical synergy in nanoparticle brushes with grafted gradient copolymers is illustrated in Fig. 9c. P(MMA-*grad*-BA) exhibits self-healing properties and excellent mechanical properties compared to alternating and random copolymers, where the level of nanophase separation heterogeneity in gradient polymer nanocomposites can be highly regulated.

Building upon previous research, Zhao et al. [98,99] investigated the influence of sequence structure on the self-healing and shape memory properties of SiO_2-*g*-PMMA-*grad*-PBA and SiO_2-*g*-PBA-*grad*-PMMA copolymer brush particle films based on the "topology-induced heterogeneity" of gradient polymer brushes, which are illustrated in Fig. 9a and b. The sequence structure has significant influence on the self-healing and shape memory properties of copolymer brush materials. Because of its uniform microstructure, the material of statistical sequence exhibits more free chain movement, which promotes the reconstruction between fracture surfaces and has faster self-healing speed. Brush particle materials exhibit unique cooperative relaxation characteristics due to their complex microstructure. The extensive coupling between the internal entanglement network and the quasi-static particle core plays a significant role in this behavior. This coupling slows down the diffusion, displacement and flow over large scales. As a result, these materials demonstrate substantial advantages in shape recovery.

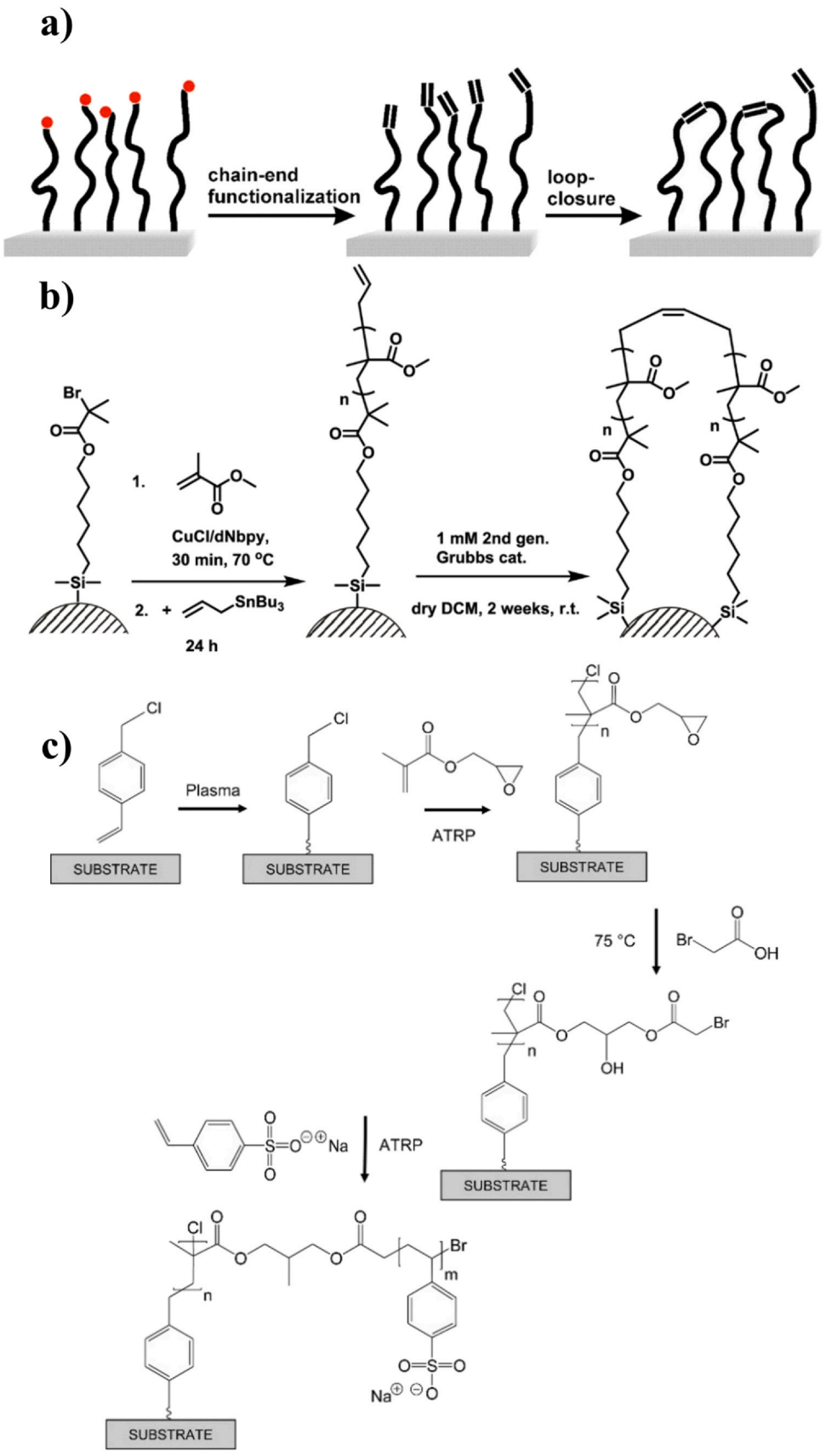

Fig. 8. a) Synthesis of loop-type polymer brushes via chain-end functionalization and subsequent loop-closure metathesis. b) Synthesis of loop PMMA brushes *via* SI-ATRP of MMA and subsequent chain-end modification and loop-closure metathesis. c) Poly(glycidyl methacrylate) brushes grafted by ATRP onto plasma-deposited poly(vinylbenzyl chloride) initiator layers, followed by the esterification of poly(glycidyl methacrylate) with bromoacetic acid to form tethered macroinitiator sites for the subsequent ATRP of poly(sodium styrene sulfonate) side-chain "bristles".
(a,b) Reproduced with permission from Ref. [89]. Copyright 2019 American Chemical Society. (c) Reproduced with permission from Ref. [90]. Copyright 2011 American Chemical Society.

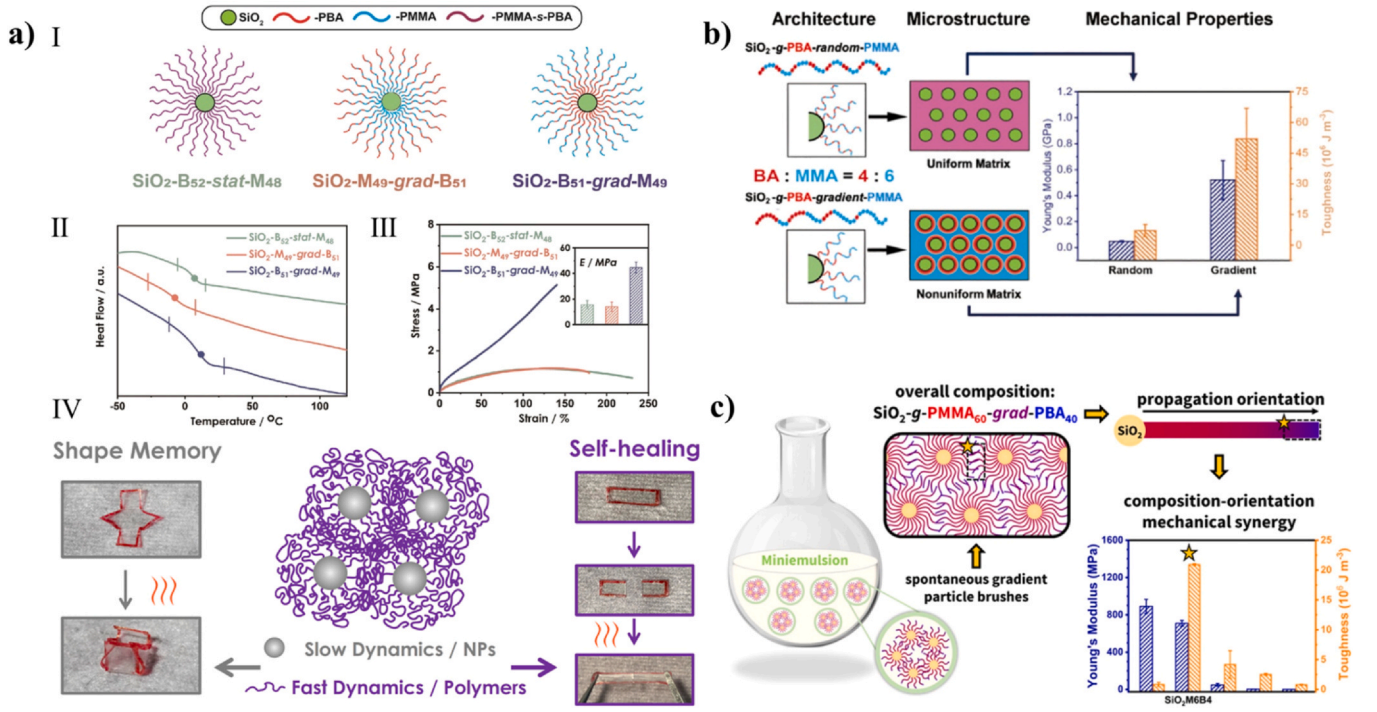

Fig. 9. a) (I) Illustration of chain architecture in particle brush systems. (II) Differential scanning calorimetry heat flow curves; the positions of T_g's are highlighted with solid points in the figures. The onset and offset points of the glass transitions are highlighted in the figures. Measurements were performed at the third eating cycle at a heating rate of 20 °C. (III)Strain-tress curves; inset: Young's modulus calculated from the incipient slope of strain stress curves. Measurements were performed at a strain rate of 0.05 mm/s. (IV) Schematic illustration of shape-memory and self-healing test. b) Schematic illustration of topologically induced heterogeneity in gradient copolymer brush particle materials. c) Schematic illustration of composition-orientation induced mechanical synergy in nanoparticle brushes with grafted gradient copolymers.
(a) Reproduced with permission from Ref. [99]. Copyright 2023 American Chemical Society. (b) Reproduced with permission from Ref. [98]. Copyright 2022 American Chemical Society. (c) Reproduced with permission from Ref. [97]. Copyright 2023 American Chemical Society.

Polymer brushes can also be synthesized to form more complex polymer topologies, e.g. binary mixed [100], bimodal [101] or Y-shaped [77].

A binary homopolymer brush consists of two different types of non-miscible polymers grafted from the same surface in a random or alternating fashion. If both types of polymer brushes are well-controlled and have narrow distributions, the binary brush approach can also be employed to prepare polymer brushes with bimodal distributions. Common synthesis approaches utilize Y-shaped initiators, tailored to orthogonally activate the corresponding initiator in unique reaction conditions to enable the development of asymmetric Y-shaped brushes with distinct polymers on each branch. e.g., combining ATRP initiators with NMP initiators [77,102], ring-opening metathesis polymerization /ATRP, ATRP/photo-iniferter-mediated polymerization, ATRP/RAFT polymerization and ATRP/conventional free radical polymerization. Jiang et al. [77] grafted symmetrical bifunctional initiators (Y-initiators) onto the surface of silica nanoparticles, and synthesized a series of high-grafting-density hybrid P*t*BA/PSt brushes *via* consecutive ATRP of *tert*-butyl acrylate and NMP of styrene. Because the bifunctional initiators increase the number of initiation sites per unit area, the total grafting density of the resulting mixed brushes is 0.9–1.2 chains/nm^2, substantially higher than the grafting density of mixed brushes grafted from functionalized silica particles with Y-initiators terminated with one chlorosilane (0.6–0.7 chains/nm^2), which is illustrated in Fig. 10. Other methods include repeated surface functionalization, partial deactivation of growing chains, extending chains with different reactivities from chain ends, and partial refunctionalization of chains that ends with a mixture of initiators and "dummy" initiators, as illustrated in Fig. 11 [6].

Based on surface-initiated methods, bimodal polymer brushes can be obtained by controlling the termination or extension of the polymer brush end groups and post-polymerization patterning methods (Fig. 10) [6]. Yan et al. [103] prepared the first layer of short and dense polymer brushes from silica nanoparticles by grafting based on ATRP, followed by employing various end-group modification methods to control the termination or regeneration of the polymer brush end-groups. One strategy involved adding 2,2,6,6-tetramethylpiperidoxyl or nucleophiles to partially deactivate halide chain ends of the grafted chains before chain extension, resulting in the preparation of polymer brushes with bimodal distributions. Additionally, copper-catalyzed azide-alkyne cycloaddition click chemistry was employed after the substitution of bromide chain ends with azides. At similar inorganic contents, crazing was observed in particle brushes with bimodal MWD, demonstrating the effectiveness of interparticle entanglement, in contrast to its unimodal counterpart. It was proposed that grafting polymer brushes with bimodal MWDs is promising in preparing robust matrix-free hybrid materials (Fig. 12).

Furthermore, another approach to preparing bimodal polymer brushes via SI-ATRP is to combine this technique with standard photolithography or microcontact printing. These methods facilitate the direct initiation of polymerization and enable the formation of predefined patterns through external stimuli [104]. Wang et al. [81] grafted PMMA with different grafting densities from the surface of silica as the first block, followed by ARGET ATRP chain extension to synthesize the PSt segment, as shown in Table 1. Under conditions of low concentrations of SiO_2-*g*-PMMA–Br macroinitiator, the efficiency of chain expansion was affected by insufficient end-chain activity. The reduced grafting density allowed for more efficient interactions between the chains of the block copolymer, resulting in a microphase separation (M-*b*-S-1, Fig. 13(b-I)). Besides, with higher macroinitiator concentrations and higher chain expansion efficiencies, more discrete "particle strings" were observed (M-*b*-S-4, Fig. 13(b-IV)). The system

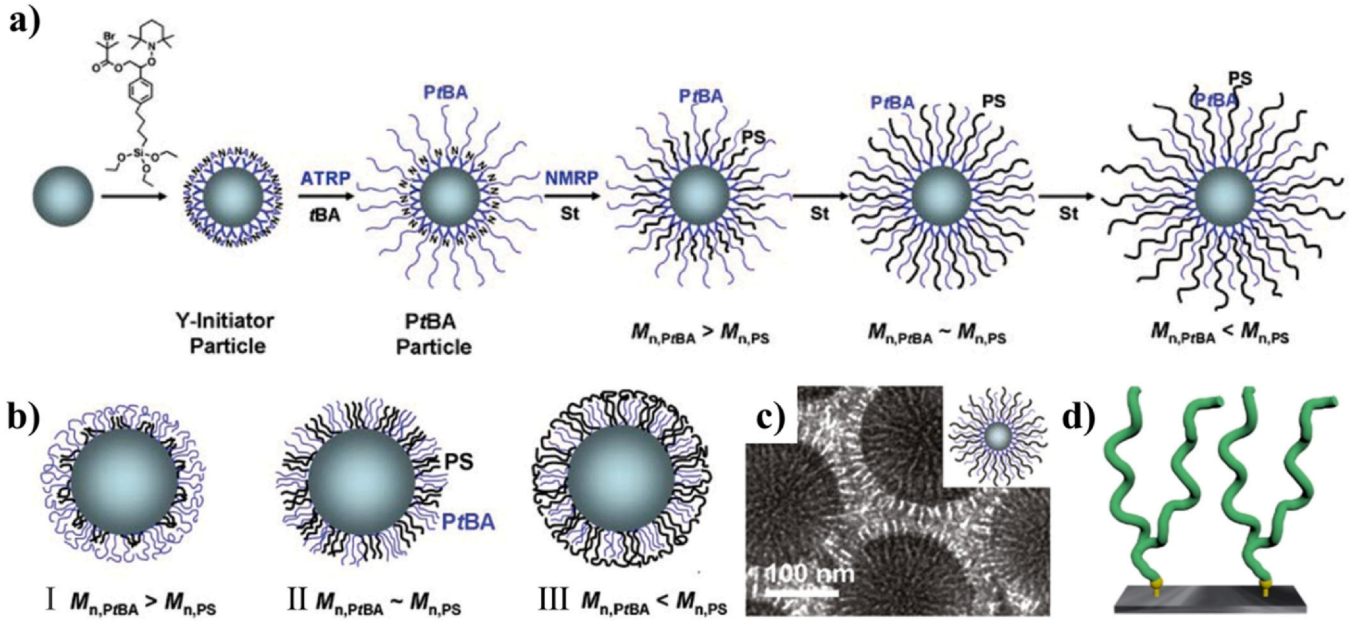

Fig. 10. a) Schematic illustration for the synthesis of high grafting density mixed P*t*BA/PSt brushes with a fixed P*t*BA M_n and various PSt molecular weights by sequential ATRP and NMRP from Y-initiator-functionalized silica particles. b) Schematic illustration of microphase separation of high density mixed P*t*BA/PSt brushes with P*t*BA M_n (left)higher than, (middle) comparable to, and (right) lower than that of PSt M_n. c) Top-view bright field transmission electron micrographs. d) Y-shaped polymer brushes.
(a,b,c) Reproduced with permission from Ref. [77]. Copyright 2010 American Chemical Society. (d) Reproduced with permission from Ref. [91]. Copyright 2020 Elsevier.

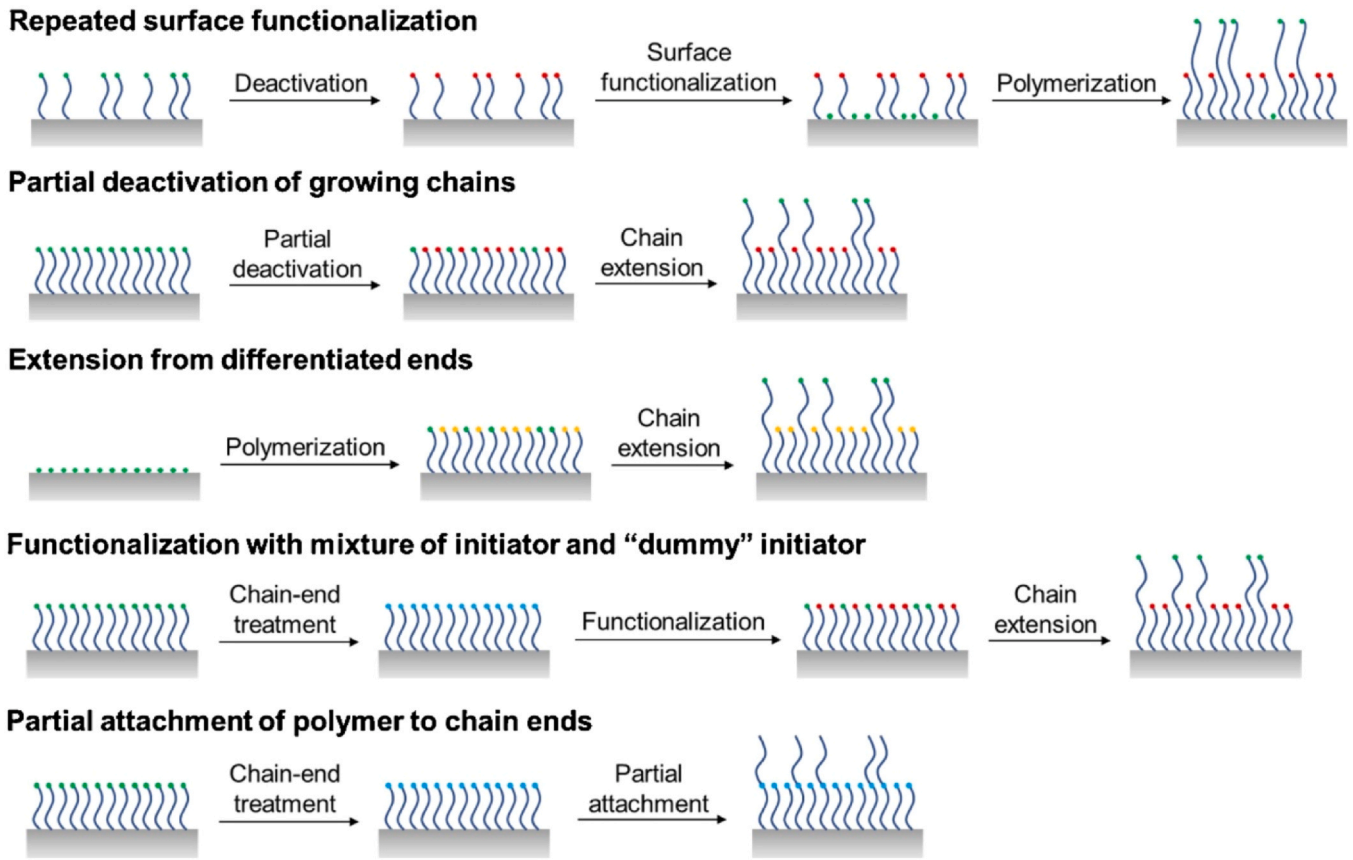

Fig. 11. Exemplified strategies for synthesis of polymer brushes with bimodal MWD by grafting from surfaces. Red: dead chain end; green: living chain end; yellow: chain end with lower reactivity; blue: other reactive functionality, e.g. alkyne, azide, etc. Adapted with permission from Ref. [6]. Copyright 2019 Elsevier.

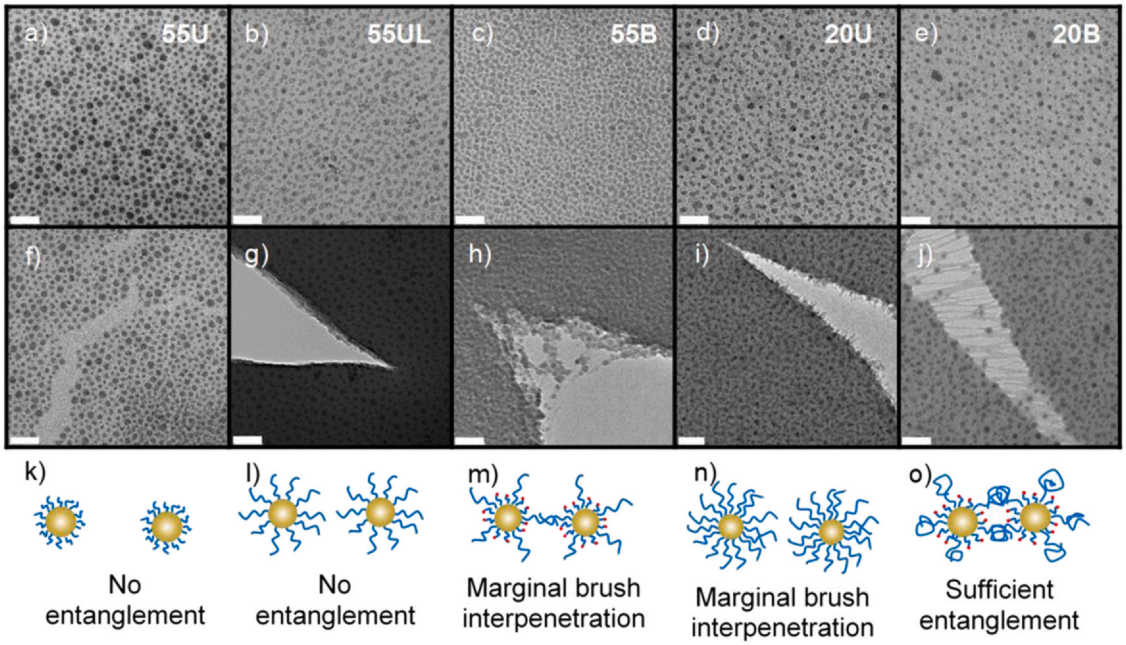

Fig. 12. Bright field TEM images of approximate monolayers (a-e), crack formation (f-j) and illustrations of cracks (k-o) of the five samples. All scale bars: 100 nm. Unimodal sample 55 U (SiO_2-*g*-PSt_{80}, a, f, k): $N < N_e \sim 160$, extensive crack propagation. Unimodal sample 55UL (SiO_2-*g*-PSt_{170}, b, g, l): above entanglement limit but in CPB regime (DP < 250), sharp crack formation. Bimodal sample 55B (SiO_2-*g*-*bi*-$PSt_{13,170}$, c, h, m): long brushes above entanglement limit and slightly beyond CPB/SDPB transition ($\sigma_l \sim 0.11$ chains/nm^2), plastic deformation. Unimodal sample 20 U (SiO_2-*g*-PSt_{250}, d, i, n): $N > N_e$ and slightly beyond CPB-SDPB transition, stent-like undulation formation. Bimodal sample 20B (SiO_2-*g*-*bi*-$PSt_{69,790}$, e, j, o): long brushes in SDPB regime and far above entanglement limit, craze formation. Scale bars = 100 nm. Adapted with permission from Ref. [103]. Copyright 2015 American Chemical Society.

Table 1
Result of syntheses of SiO_2-*g*-PMMA and SiO_2-*g*-PMMA-*b*-PSt particle brushes with different grafting density and compositions.

Entry[a]	M_n[b]	M_n/M_w[b]	f_{ino}(%)[c]	σ(chains/nm^2)[d]	f_{PMMA}(%)[e]	σ_1(chains/nm^2)[f]	$f_{PMMA\text{-}b\text{-}PSt}$(%)[e]	σ_2(chains/nm^2)[f]
M-*b*-S−1	209,400	2.66	24.52	0.049	93.1	0.043	6.9	0.003
M-*b*-S−2	241,800	2.11	24.15	0.044	88.6	0.039	11.4	0.005
M-*b*-S−3	206,800	3.17	27.52	0.042	45.2	0.019	54.8	0.023
M-*b*-S−4	80,600	1.68	21.98	0.043	19.7	0.008	80.3	0.035
M-*b*-S−5	97,100	2.46	5.3	0.609	68.5	0.417	31.5	0.192
M-*b*-S−6	113,000	1.93	15.8	0.156	54.9	0.086	45.1	0.070
M-*b*-S−7	152,400	4.41	36.7	0.038	70.6	0.027	29.4	0.011

[a] Reaction conditions: PMMA-L1–2: $[MMA]_0/[SiO_2–Br]_0/[CuCl_2]_0/[dNbpy]_0/[CuCl]_0$ 3000:1/4:0.4:8:3.6; PMMA-H1/M1/L3: $[MMA]_0/[SiO_2–Br]_0/[CuCl_2]_0/[dNbpy]_0/[CuCl]_0$ 4000:1:0.4:8:3.6; M-*b*-S-1–2: $[S]_0/[PMMA\text{-}L1]_0/[CuBr_2]_0/[Me_6TREN]_0/[Sn(EH)_2]_0$ 50,000:1/2:5:50:5; M-*b*-sS-3–4: $[S]_0/[PMMA\text{-}L2]_0/[CuBr_2]_0/[Me_6TREN]_0/[Sn(EH)_2]_0$ 5000:1/2:0.5:5:0.5; M-*b*-S-5–7: $[S]_0/[PMMA\text{-}H1/M1/L3]_0/[CuBr_2]_0/[Me_6TREN]_0/[Sn(EH)_2]_0$ = 10,000:1:2:20:2 with 45 vol% of anisole and 5 vol% of DMF at 60 °C.
[b] Determined by SEC.
[c] f_{ino} (inorganic content), determined by TGA.
[d] σ (grafting density), calculated according to TGA data.
[e] mol% fraction of PMMA blocks and PMMA-*b*-PSt blocks in particle brushes.
[f] Calculated according to TGA data, $\sigma = \sigma_1 + \sigma_2$.

with a high graft density of PMMA-*b*-PSt ligands (M-*b*-S-5, Fig. 13(c-I, II)) produces a relatively homogeneous structure due to the sufficient PSt outer layer. On the contrary, systems with low and medium grafting densities display highly anisotropic morphological characteristics, such as connected strings (M-*b*-S-6, Fig. 13(c-III, IV)) and continuous cluster networks (M-*b*-S-7, Fig. 13(c-V, VI)). A recent report introduced a β-diketoenamine dynamic covalent linkage to the "root" of surfaces grafted brushes. By replacement of polymer brushes with a new batch of initiators, this approach in principle has no limit on types of polymer brushes to be introduced on a surface. In addition, it allows for other surface-initiated polymerization techniques than SI-ATRP [105].

The preparation of polymer brush-based hybrid materials typically initiates with surface functionalization through the "grafting-from" method. Subsequent polymer grafting employs diverse methodologies, with higher grafting density. Through meticulous selection of reaction conditions, the structure of the grafted polymer brush can be finely tuned, thus modulating its conformation and the interactions among particle brushes, as well as between these brushes and the substrate. This versatility helps to achieve the desired performance in a targeted application.

4. Applications

SI-ATRP enables the controlled growth of polymers from surfaces, offering precise modulation of polymer structure, morphology and properties. This capability renders SI-ATRP indispensable across a spectrum of applications. The flexible combination of polymer surfaces and structures, enabled by SI-ATRP, underscores its pivotal role in fabricating organic/inorganic quasi-one-component nanocomposites, with boundless application potential. In this section, we categorize both established and emerging application domains based on the inherent structural attributes of polymers synthesized *via* SI-ATRP, and provide forward-looking perspectives on areas ripe for further exploration.

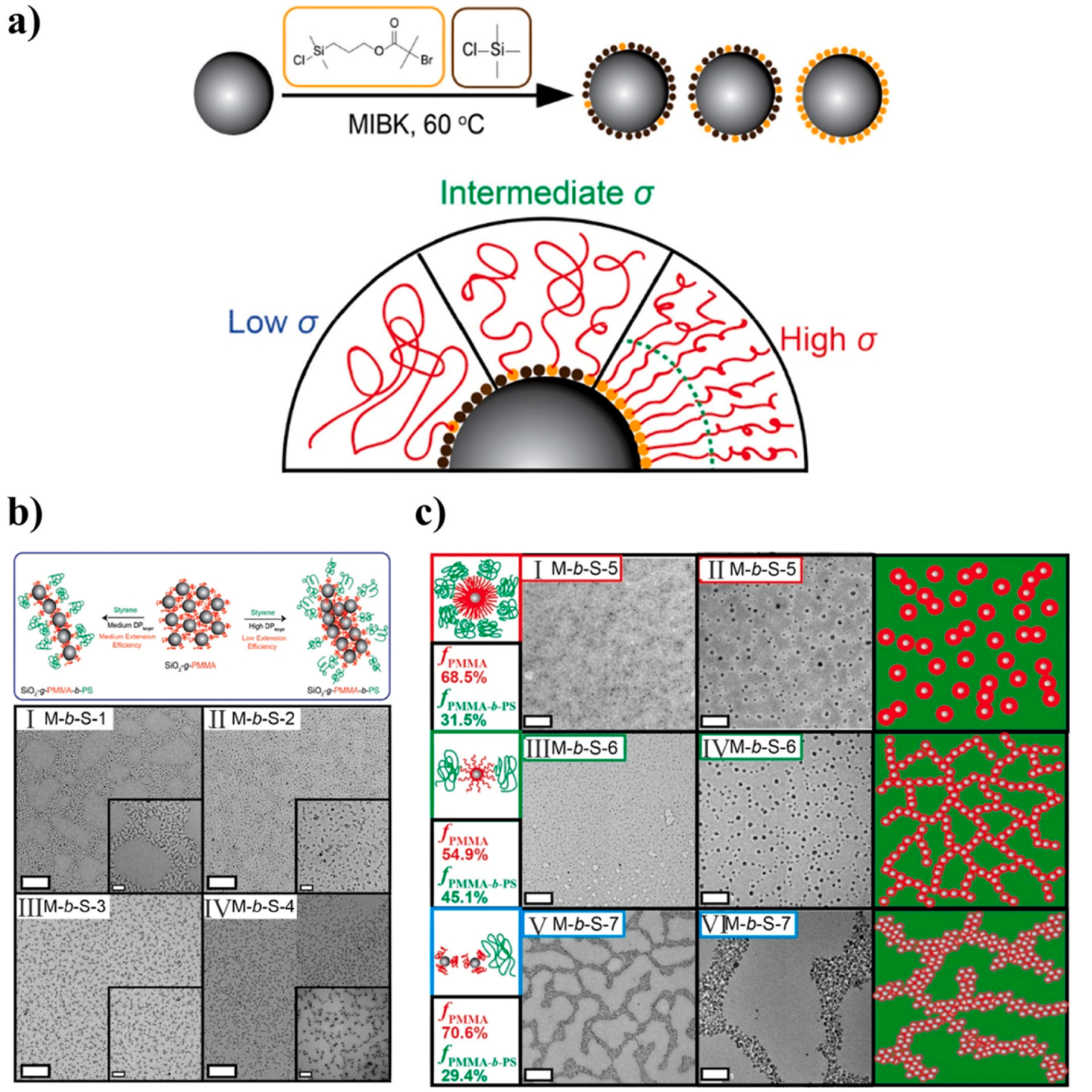

Fig. 13. a) Synthesis of SiO_2-*g*-PMMA particle brushes with different grafting densities. b) Schematic graph of the synthesis and assembly of bimodal SiO_2-*g*-PMMA/PMMA-*b*-PSt particle brushes and TEM images of SiO_2-*g*-PMMA-*b*-PSt particle brushes. (I) M-*b*-S-1, (II) M-*b*-S-2, (III) M-*b*-S-3 and (IV) M-*b*-S-4. Scale bar: 500 nm. Inset scale bar: 100 nm. c) TEM images of SiO_2-*g*-PMMA-*b*-PSt particle brushes. (I, II) M-*b*-S-5, (III, IV) M-*b*-S-6, (V, VI) M-*b*-S-7. Scale bar: (I), (III), (V), 500 nm; (II), (IV), (VI), 100 nm. Reproduced with permission from Ref. [81] Copyright 2020 American Chemical Society.

4.1. Improvement of mechanical properties

The primary intention behind the design of organic/inorganic composites is to enhance the physical and mechanical properties of polymeric materials [106,107], as well as the processing and application performance of inorganic materials [108]. SI-ATRP aligns with this objective. Consequently, a considerable body of research has focused on optimizing the dispersion state of nanoparticles and the microstructure of polymers through the molecular design of polymer structures, ultimately strengthening the macroscopic physical properties of polymer brush-grafted nanoparticles [109]. By modulating various aspects of polymer chain structure (e.g. composition, polymerization degree, grafting density and topological structure), manipulating crystalline structure [110] and exploiting interactions between organic and inorganic components [111], comprehensive enhancements in physical performance have been achieved. These enhancements include superior tensile properties induced by the physical entanglement of polymer brushes [97], ideal dynamic mechanical properties resulting from interactions between polymer chains and inorganic nanoparticles [111], outstanding processability conferred by polymer chain-modified inorganic fillers [112] and self-healing properties provided by specific structures such as hydrogen bonds [99,113]. These polymer products

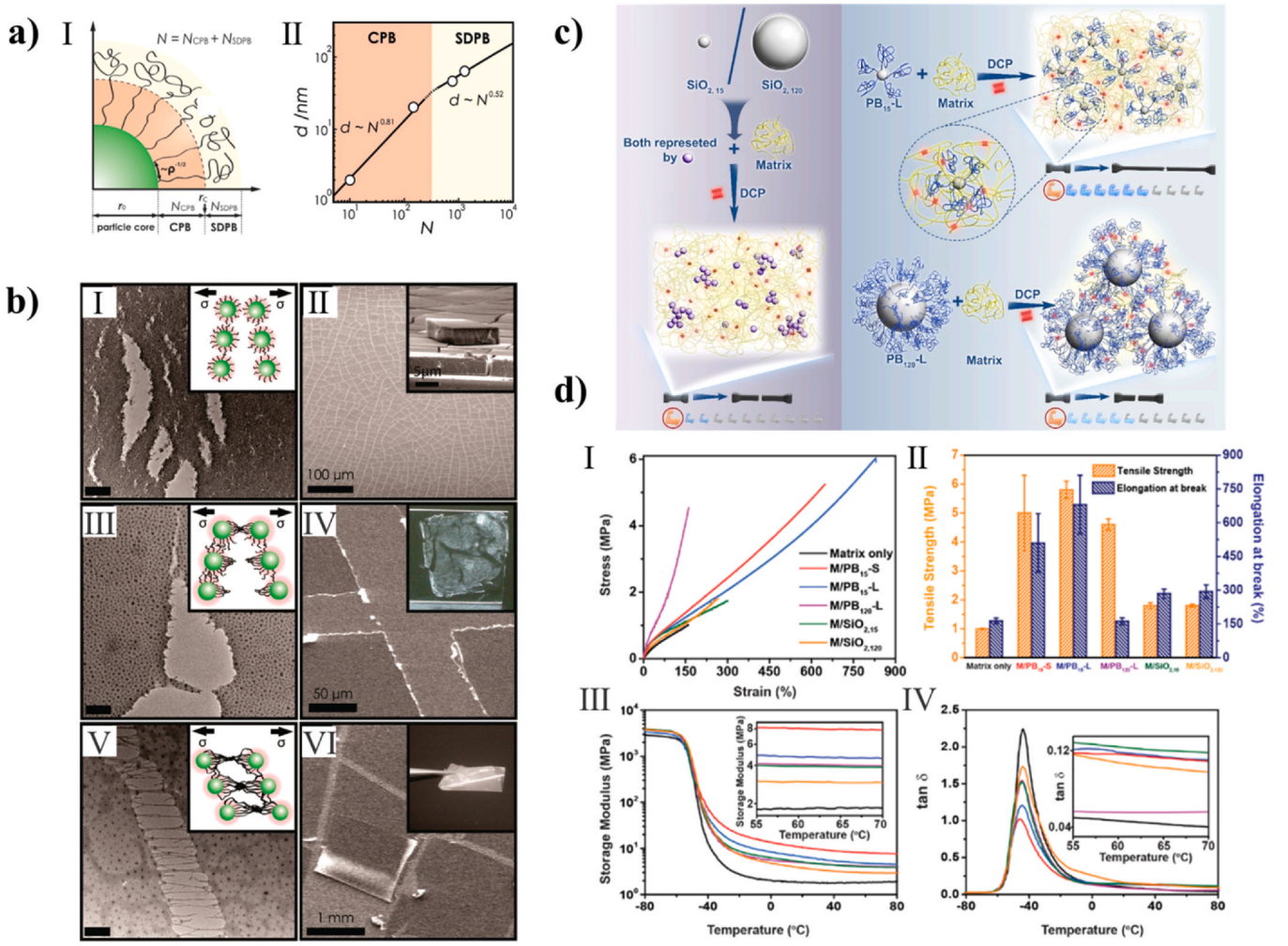

Fig. 14. a) (I) Illustration of CPB (red) and SDPB (yellow) regimes. (II) Dependence of particle surface-to-surface distance d on the degree of polymerization N of polymer grafts determined by TEM of particle monolayers (not shown). The scaling of the chain end-to-end distance $R_E \sim N^x a$ of grafted chains is $x = 0.81$ (CPB) and $x = 0.52$ (SDPB). Colored regions correspond to predicted particle brush regimes. b) Deformation characteristics of particle film assemblies. (I) Brightfield transmission electron micrograph (TEM) revealing multiple crack formation in SiO_2-St_{10} thin (~50 nm) films. Inset illustrates crack formation normal to acting stress direction. (II) Crack pattern in SiO_2-St_{10} thick (~5 μm) film after solvent evaporation. Inset shows magnification. (III) Crack formation in thin (~50 nm) film of SiO_2-St_{10}. Stent-like undulations form across the fracture surface. Inset illustrates crack formation. (IV) Scanning electron micrograph (SEM) of scratched thick (~5 μm) film depicting wax-like deformation. Inset shows image of free-standing film (~50 μm) revealing fragile characteristics. (V) TEM of fracture crack in thin film of SiO_2-St_{770} (approximately monolayer). The formation of fibrils is observed that "bridge" particle cores across the fracture surface. Inset illustrates proposed mechanism of fibril formation by entanglement of relaxed chain segments in the SDPB regime. (VI) SEM of scratched thick (~5 μm) film of SiO_2-St_{770}, revealing peeling of film. Inset shows flexible deformation of free-standing film (~50 μm). Scale bar in panels a, c and e is 200 nm. c) Schematic illustration of SiO_2-*g*-Polyisoprene particle brush reinforced advanced elastomer nanocomposites prepared *via* ARGET ATRP. d) (I) Stress-strain curves of cured PI and PI/SiO_2 nanocomposites, (II) Plots of the tensile strength and elongation at break of cured PI and PI/SiO_2 nanocomposites, (III) Storage modulus G' (inset: G' from 55 to 70 °C), (IV) loss factor tan δ (inset: tan δ from 55 to 70 °C) for M/SiO_2 and M/PB nanocomposites, black: matrix only, red: M/PB_{15}-S, blue: M/PB_{15}-L, magenta: M/PB_{120}-L, olive: M/$SiO_{2,15}$, orange: M/$SiO_{2,120}$.
(a,b) Reproduced with permission from Ref. [115]. Copyright 2010 American Chemical Society. (c,d) Reproduced with permission from Ref. [43]. Copyright 2024 Wiley.

with tailored performance improvements have potential applications in aerospace, automotive manufacturing, shipbuilding and other industrial sectors as novel high-performance materials, including green tires, modified fillers and modified carbon fibers.

In the fabrication of one-component nanocomposites using hybrid particles, the grafting density and polymerization degree of the grafted chains exert direct influence on the interactions and stacking behavior of the hybrid particles [114]. The entanglement of grafted chains can enhance the toughness and flexibility of the bulk material. Fig. 14a illustrates the conformation of chains [115], showing stretched conformations near the particle surface, while relaxed conformations are observed when the particle brush size exceeds the critical radius. Studies using nanoindentation techniques on PSt and PMMA-grafted silica nanoparticles indicate that an increased degree of polymerization in the grafted chains correlates with enhanced elastic modulus. This enhancement is attributed to the strengthened interactions among the grafted polymer chains [108]. Moreover, a significant increase in the toughness of the brush films is observed in the SDPB system, attributed to the formation of relaxed regions between chains that facilitate the ordered arrangement of particles during stretching and relaxation processes. The illustration of CPB and SDPB regimes is shown in Fig. 14a. The relationship between the degree of polymerization N and the particle surface-to-surface distance d determined by TEM of particle monolayers is depicted in Fig. 14b. Kubiak et al. [116] grafted poly (methyl methacrylate-*co*-glycidyl methacrylate) from the surface of silica, where the epoxy residues in the system could undergo reactions

with multifunctional amines to achieve inter-particle covalent cross-linking. This resulted in nanocomposites with excellent mechanical properties and high loading efficiency of inorganic particles. Zhao et al. [44] grafted ultra-high molecular weight polyisoprene(PI) from the surface of nano silica. As the polymerization degree of the grafted chains increased, both the mechanical strength and toughness of the material improved. This enhancement can be attributed to denser entanglements, resulting in higher storage modulus of the material.

Hybrid particles, serving as functional fillers, exhibit dispersed morphologies in the polymer matrix that are influenced by the grafting density of the grafted chains, the polymerization degree of the grafted chain and the polymerization degree of the matrix. Hybrid particles with high grafting density and long grafted chain lengths were found to be in a phase-separated state or well-dispersed state. However, hybrid particles with relatively low grafting density and shorter grafted chain lengths formed a series of structures within the polymer matrix due to core-shell interactions, including string-like, sheet-like and small clusters [117,118].

Wu et al. [111] adjusted the interaction parameters by selecting different solvents, enabling rapid switching between phase-separated and homogeneous states of particle brushes through direct annealing. The specific dispersion state of nanoparticles is crucial for optimizing the specific properties of nanocomposites. The assembly of particle brush fillers into linear or sheet-like structures transcends the constraints of traditional dispersion morphologies, as defined by homogeneous theory. This approach unlocks new opportunities for modifying the mechanical and transport properties in particle brush/polymer blend systems, offering advanced capabilities beyond conventional configurations.

We have recently achieved SI-ATRP of isoprene from the surface of nanosized silica for the first time, by designing and preparing highly designable and high-performance SiO_2 hybrid particle brushes. Besides, linear PI was synthesized through ATRP as a matrix. SiO_2-*g*-PI/PI rubber nanocomposites with excellent service performance were prepared, which improved the dispersibility of SiO_2 and the mechanical properties of the composite materials. The loss factor of SiO_2-*g*-PI/PI rubber nanocomposites at 60 ℃ decreased from 0.107 to 0.056, with the silica core particle size being 120 nm. This technique offered a new design approach and breakthrough for the next generation of green tires which meet the Carbon Neutrality targets with low rolling resistance (Fig. 14c,d) [43].

In addition to the monomodal particle brush, the bimodal particle brush as fillers in the preparation of nanocomposites provide a pathway to achieve particle brush/matrix dispersions with high inorganic content and athermal systems (grafts that have the same chemical composition as the matrix), by reducing both particle core–core attractions with high grafting density brushes and entropic penalty for the matrix penetrating into the brush with low graft density brushes [119]. In a system without a matrix, the bimodal particle brush system provides entanglement and higher fracture toughness to the material through high-molecular weight side chains [103].

4.2. Responsive materials

One of the advantages of SI-ATRP is the flexibility and diversity of monomers, allowing for the introduction of responsive functional units exhibiting a change in their conformation (different entanglement states of polymer chains and variations in interparticle distances), surface energy, or charge state, triggered by an external stimulus such as temperature [120], pH [121,122], biosignal [123], light [124] or mechanical stress. A significant amount of research on smart responsive devices is based on this feature [125]. Monomers sensitive to temperature/pH, when polymerized *via* ATRP, could find wide applications in environment monitoring in water, air, soil and other media [126]. Chakraborty et al. [127] grafted thermoresponsive polymers brushes from 20 nm colloidal gold *via* ATRP of *N*-isopropylacrylamide (NIPAM). The system exhibited thermal-responsive behavior across its lower critical solution temperature. Monomers sensitive to photoelectric signals, when polymerized via ATRP, are applied in the development of flexible wearables and smart devices [128]. Research has also extended to CO_2-responsive monomers for SI-ATRP polymerization [129], where the synthesized nanohybrids have been successfully employed in gas detection and controlled release, thereby providing new insights into applications of SI-ATRP in sustainable development.

Another category of highly specialized yet extensively utilized materials comprises magnetic nanoparticles grafted with polymer brushes, which exhibit magnetic responsiveness originating from the nanoparticles. Employing low-toxicity, high-magnetization nanoparticles such as magnetite (Fe_3O_4) or maghemite (γ-Fe_2O_3) as the core, they respond to tailored magnetic stimuli. Through polymer grafting from the surface of magnetic nanoparticles, inorganic magnetic nanoparticles acquire excellent mechanical properties and diversified functionalization, enabling their wide-ranging applications in resonance imaging [59], drug delivery [130], tissue engineering [131], liquid separation [132] and various other domains. Similar to other inorganic nanofillers, magnetic nanoparticles also tend to aggregate driven by low surface energy, thereby affecting the uniform grafting of polymer chains. However, employing techniques such as ultrasonication facilitates the preparation of well-dispersed magnetic nanoparticle-grafted with polymer brushes, signifying their importance in developing novel functional nanomaterials with customized properties. Dehsari and Asadi [133] reported the ultrasound-mediated surface-initiated atom transfer radical polymerization (uSI-ATRP) for grafting PMMA from nanoparticles, followed by solution casting the particle brushes into films. Individual nanoparticles were uniformly dispersed within the films, exhibiting well-controlled packing densities. Moradi et al. [134] functionalized the surface of magnetic Fe_3O_4 nanoparticles with chloroacetyl chloride and subsequently initiated ATRP of NIPAM to graft PNIPAM from the nanoparticles. Further, they grafted deacetylated chitosan onto the polymer brushes. PNIPAM and chitosan served as the thermo-responsive and pH-responsive segments, respectively, resulting in a novel hybrid material with triple responsiveness to temperature, pH and magnetic field for cancer drug delivery (Fig. 15). This work had potential applications in preparing multi-responsive vectors and advancing precision medicine.

Heidari et al. [135] developed a novel colorimetric sensor for the naked-eye detection of multiple ions in aqueous solutions by polymerizing acrylamide, *N,N*-methylenebisacrylamide (MBA) and dithizone (diphenylthiocarbazone, DTZ) monomers from modified TiO_2 nanoparticles using ATRP. In this system, DTZ is employed as a chromogenic agent due to its high selectivity and sensitivity for heavy metal ions, while acrylamide addresses the poor aqueous solubility of DTZ, and MBA serves as a cross-linker, enabling effective adsorption of heavy metal ions even at low ion concentrations. The sensor exhibits a rapid response time of 30 s with a detection limit of 10 ppb for mercury (II), 1 ppb for cadmium (II), 0.5 ppb for Cu (II) and 1 ppb for Uranium dioxide (II). Through a colorimetric approach, the sensor can selectively identify target ions in the presence of various interfering ions by observable color changes (e.g., gray to violet, orange, green and yellow). The sensor demonstrates excellent reversibility, stability and a short response time, offering multi-target ion detection over a wide dynamic range and proving suitable for rapid analysis of real water samples. Diepenbroek et al. [136] present a straightforward method for fabricating films composed of stacked PNIPAM-grafted silica nanoparticles. The material exhibits distinct and reversible color changes in the presence of near-saturated ethanol vapor, a stimuli-responsive structural color property that is successfully utilized for ethanol vapor sensing. Due to the high affinity of PNIPAM for ethanol, the coatings showed a rapid response to ethanol vapor, exhibiting a pronounced swelling effect that results in a measurable change in thickness. The experimental results indicate that the sensor has high sensitivity to ethanol vapor (with a detection limit as low as 10 ppm), a fast response time (on the order of seconds) and good reversibility, allowing for repeated use. The sensor also exhibited superior selectivity for ethanol vapor compared to other organic solvents. These findings suggest that PNIPAM-based sensors have significant potential for *ex-situ* ethanol vapor detection, particularly in applications that require rapid, cost-effective and repeatable measurements.

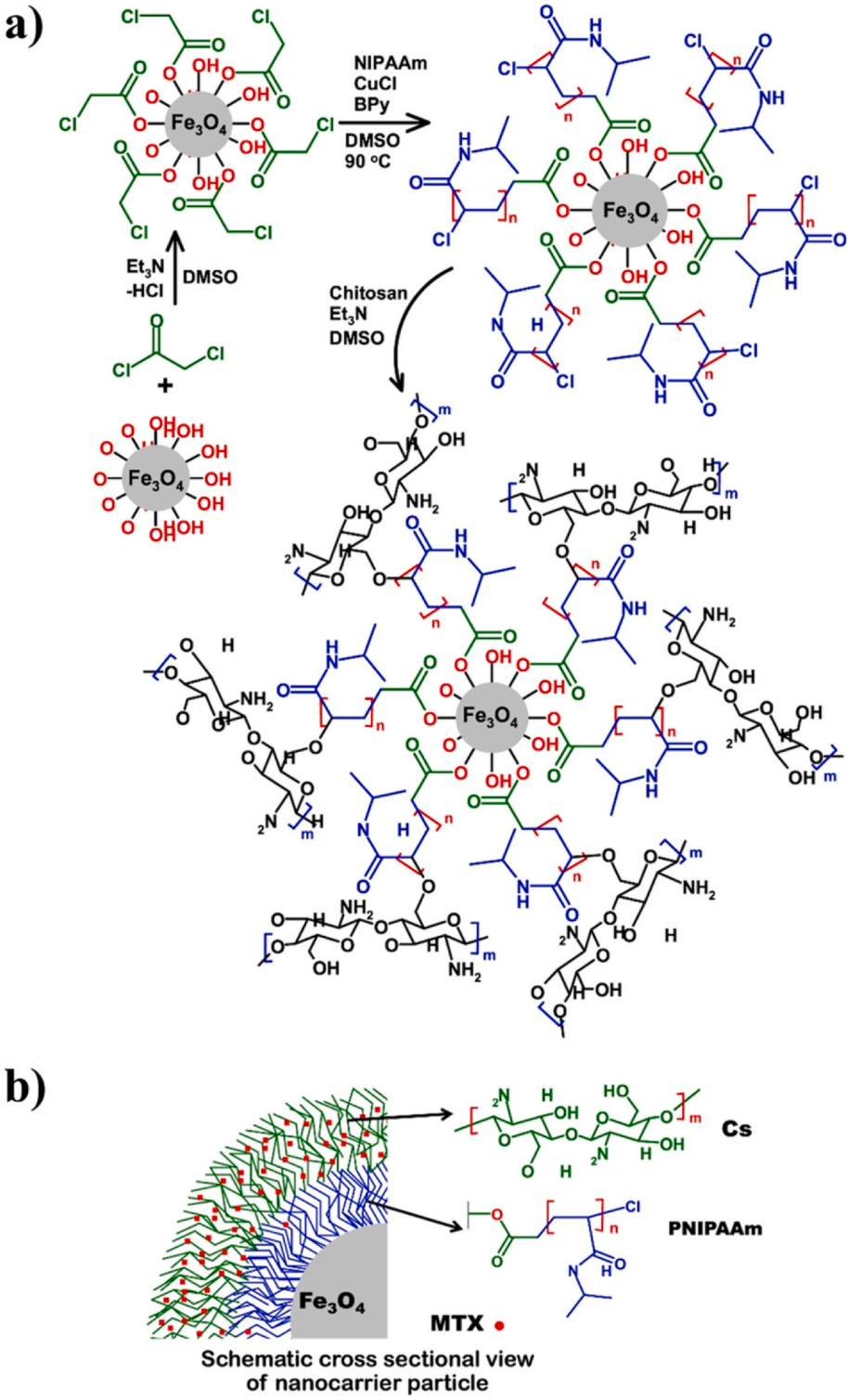

Fig. 15. a) The reaction route for the synthesis of Fe_3O_4-chloroacethyl@PNIPAM-*g*-chitosan core-shell magnetic nanoparticles (a typical possible structure) and b) Schematic illustration of the possible structure for a prepared nanocarrier particle. Reproduced with permission from Ref. [134]. Copyright 2022 Elsevier.

4.3. Energy-related and dielectric materials

Future energy storage materials require primarily a high dielectric constant and robust breakdown strength to meet performance demands effectively. Traditional polymers often exhibit high breakdown strength but low dielectric constant, while inorganic particles may possess high dielectric constant but low breakdown strength [137]. Therefore, research on the preparation of high-performance hybrid energy storage materials combining inorganic nanoparticles/polymer brushes *via* SI-ATRP has been receiving considerable attention. Similar to other application scenarios, the aggregation of nanoparticles can lead to uneven dielectric performance and premature material failure [138]. Effective promotion of the compatibility between the nanoparticles and the matrix have been achieved by grafting polymer brushes *via* SI-ATRP. This approach is a key pathway to enhancing the dielectric performance of materials. Apart from the uniform dispersion of nanoparticles,

excellent interfacial properties between the polymer and the nanoparticles are also crucial [139]. In terms of preparation, unlike other materials, the selection narrows to inorganic nanoparticles with high dielectric constant (high κ), such as $BaTiO_3$ [140], TiO_2 [141], ZrO_2, Al_2O_3 [48] and others. Xie et al. [142] first grafted hyperbranched aromatic polyamide (HBP) from the surface of $BaTiO_3$ nanoparticles, followed by the polymerization of PMMA shell using hyperbranched amine polyamide *via* SI-ATRP, to synthesize core@double-shell structured PMMA@HBP@$BaTiO_3$ nanocomposites. The prepared PMMA@HBP@$BaTiO_3$/PMMA nanocomposite exhibits a high dielectric constant (39.3) and low dielectric loss (0.0276), superior to pure PMMA and $BaTiO_3$@HBP/PMMA. The double-shell structure of PMMA@HBP@BT provided an alternative method for preparing nanocomposites with high dielectric constant and low dielectric loss.

SI-ATRP also finds applications in electrochemical sensors, supercapacitors and electrocatalysts [143]. Among these, electrochemical sensors are capable of amplifying electrical signals through grafting electroactive polymers containing a large number of redox centers [144], thereby enhancing sensor sensitivity.

Modification of carbon materials *via* ATRP, by grafting hydrophilic polymers from carbon surfaces, stabilizes capacitor performance and can even enhance capacitance. It also improves the dispersibility and processability of carbon materials. Albarghouthi et al. [58] addressed the issue of signal drift in electrochemical biosensors by grafting POEGMA from the surface of carbon nanotubes. This overcame the charge screening and drift-related limitations of biosensors. In high ionic strength solutions (1X PBS), the POEGMA shell increased the Debye length and mitigated the signal drift effect, enabling stable and repeatable detection of sub-femtomolar concentrations of biomarkers. Modifying a carbon electrode with hydrophilic polymer brushes such as poly(*N*-vinylpyrrolidone) obtained electrode materials with high specific capacitance of 279 F/g, excellent rate capability and good cycling stability, offering broad prospects in the field of energy conversion and storage [145]. Khan et al. [146] utilized poly(ethylene oxide) as a matrix and (i) graphene oxide (GO), (ii) GO-*g*-PEG_{6k} and (iii) GO-*g*-PEG_{6k}-*b*-P(MA-POSS) as fillers to prepare a series of solid polymer nanocomposite electrolytes. By comparing the particle conductivity of the composite materials prepared with GO and GO-*g*-PEG_{6k} at 50 °C, it was determined that particle brush fillers were more effective in enhancing ion conductivity. However, for the GO-*g*-PEG_{6k}-*b*-P(MA-POSS) filler, the dangling POSS nano-cages likely increased the free volume at the interface with the matrix by increasing the chain length and ion migration rate, thereby forming low-energy ion channels at the interface, resulting in enhanced ion conductivity. This work offered a new tool for adjusting ion conductivity with potential in lithium-ion battery applications.

Nonmetallic oxides have also been extensively studied in this field. Li et al. [147] successfully prepared a hybrid coating for stabilizing lithium metal anodes by grafting polyacrylonitrile from oxygen-vacancy-rich yttria-stabilized zirconia nanoparticles. The particle brushes exhibited high solvent dispersibility, ionic conductivity ($> 10^{-4}$ S/cm @ r.t.) and Young's modulus (7.56 GPa). These properties effectively prolonged the cycle life and enhanced the safety of lithium metal batteries. This study provides a novel strategy for improving the reliability and stability of lithium metal batteries, offering significant technological support for their application in electric vehicles and other fields. Tawade et al. [148] investigated the effect of graft density and molecular weight of PMMA-grafted on barium titanate surface on the dielectric properties of particles. They synthesized particle brush with varying grafting densities ranging from 0.303 to 0.929 chains/nm^2 and possessing high molecular weights between 97,700 and 130,000. The observations indicate that particle brushes with lower grafting densities and higher molecular weights exhibit superior permittivity and enhanced dielectric strength and consequently achieve greater energy densities (approximately 5.2 J/cm^3) compared to those with higher grafting densities. This performance is likely due to their "star-polymer"-like configurations, which feature elevated chain-end densities that are known to promote electrical breakdown. These findings can serve as guiding principles for developing tunable high energy density energy storage devices. Desroches et al. [149] prepared multivalent polymer poly (2-hydroxyethyl acrylate)(P2HEA) grafted nanosilica and used it as a reinforcing filler for 3D printed self-healing elastomers. The resin matrix is a statistical copolymer of 2HEA and *n*-BA. The polymer brush restructures the network by dynamically covalently reacting with the surrounding polymer matrix, the reversible interactions between the polymer chains on the nanoparticles and the elastomer matrix facilitated efficient self-healing, with the material recovering up to 90 % of its original mechanical properties after damage. Moreover, the brushes increase the composite stiffness by generating a large number of non-covalent crosslinking (entanglement and hydrogen bonding) to achieve a balance of material modulus and self-healing properties. Additionally, the particle brushes-filled elastomers demonstrated excellent printability, maintaining their self-healing properties even after 3D printing. The findings suggest that using multivalent particle brushes as reinforcing fillers offers a promising approach to developing robust, self-healing and 3D-printable elastomeric materials for a wide range of applications.

4.4. Optical devices

The optical properties of inorganic nanocomposites are jointly influenced by both inorganic nanoparticles and polymers, which alter the interaction of the material with electromagnetic waves [150]. Specifically, these changes manifest in aspects such as material transparency, refractive index and cutoff wavelength, with scattering from inorganic fillers leading to a decline in the overall optical performance of nanocomposite materials [151]. The scattering intensity of nanoparticles is determined by the scattering cross-section. For optically isotropic particles within the static electric limit, the scattering cross-section depends on the particle volume and polarizability [152]. To maintain the optical properties of nanocomposites, it is necessary to avoid agglomeration of inorganic particles or to match the refractive indices of inorganic particles with polymers; thus, covalently attaching polymer chains from the surface of inorganic particles is an effective ways to achieve this goal [153]. Besides that, inorganic nanoparticles with high refractive indices are often selected, such as ZnS, ZnO and TiO_2 [154].

In order to match the refractive indices of the particles and the medium, the grafting chain structure can be precisely controlled by SI-ATRP, which further enhances the optical and mechanical properties of the nanocomposites Dang et al. [151] investigated the influence of polymeric ligands on the optical transparency of polymer-matrix composites, focusing on the specific scenario involving poly(styrene-*co*-acrylonitrile)-grafted silica particles embedded in PMMA nanocomposites. It was observed that when the effective refractive index of the hybrid particles matched that of the matrix, the particle scattering cross-section was effectively reduced by several orders of magnitude. This reduction was achieved by establishing conditions for minimizing particle scattering cross-section through polymer-grafting, which remained applicable even for large particle dimensions comparable to the wavelength of light. This approach provides a novel pathway for the fabrication of highly transparent polymer nanocomposites and holds promise for widespread application in the realm of optically engineered materials.

In addition, the application of inorganic nanoparticle/polymer brushes in optical devices involves other directions. Optical properties are altered based on polymer-grafting of nanofillers, leading to the preparation of advanced optical sensor materials. Tokareva et al. [155,156] translates pH variations in a physiologically relevant range into distinct optical signals, capitalizing on the swelling and shrinking behavior of polymers such as poly(2-vinylpyridine) and PDMAEMA combined with the localized Au surface plasmon resonance from the nanoparticles.

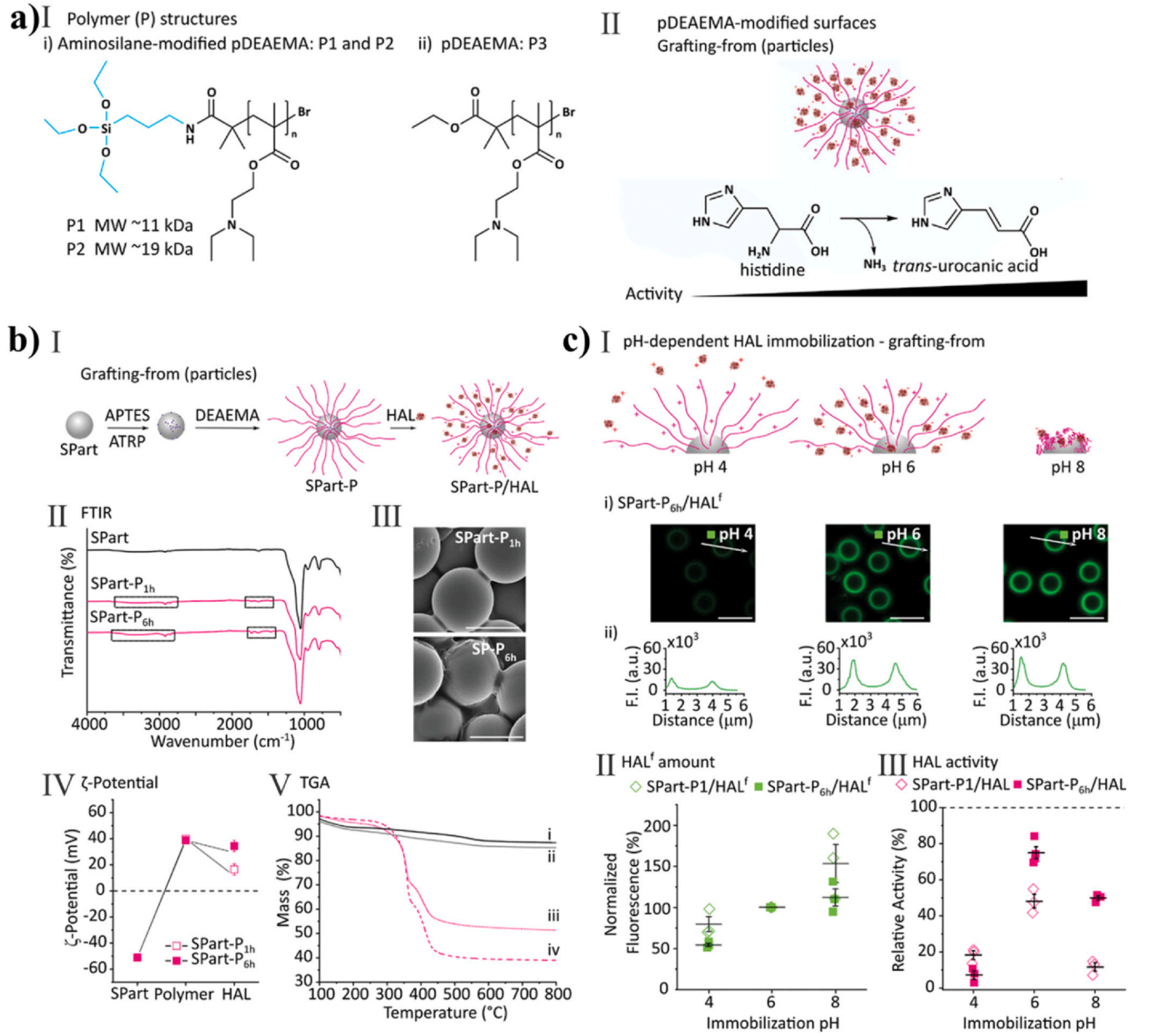

Fig. 16. a) (I) Structure of PDEAEMA including the triethoxysilane group (for P1: MW ≈ 11 kDa and P2: MW ≈ 19 kDa) for covalent attachment to silica surfaces. (II) Cartoon of particle surfaces modified with polymer brushes via the grafting-from method, including the immobilized HAL enzyme and its catalytic activity to convert histidine into *trans*-urocanic acid. b) Grafting-from on particles. (I) Cartoon of the assembly of the polymer brush-coated particles and the HAL immobilization. (II) FTIR spectra of SPart, SPart-Initiator 2, SPart-$P_{1\,h}$ and SPart-$P_{6\,h}$. The black rectangles denote the characteristic bands for the polymer. (III) Representative SEM images of SPart-$P_{1\,h}$ and SPart-$P_{6\,h}$ (scale bars: 2 μm). (IV) The ζ-potential of SPart, SPart-Initiator 2, SPart-$P_{1\,h}$ and SPart-$P_{6\,h}$, as well as of these particles after the HAL adsorption (SPart-$P_{1\,h}$/HAL and SP-Part$_{6\,h}$/HAL). Data are presented as mean ± SD. (n = 2) (V) Thermogravimetric analysis (TGA) of $^{0.5}$SPart (i), $^{0.5}$SPart-Initiator 2 (ii), $^{0.5}$SPart-P_1 (iii) and $^{0.5}$SPart-$P_{6\,h}$ (iv). c) (I) Cartoon illustrating the pH-dependent interaction of HAL with SPart-$P_{6\,h}$. Representative CLSM images of HAL^f immobilized on SPart-$P_{6\,h}$ at pH 4, 6 and 8 (i–ii) (green: HAL^f) (scale bars: 5 μm). (II) Particle mean fluorescence of SPart-P1/HAL^f and SPart-$P_{6\,h}$/HAL^f after immobilization at pH 4, 6 and 8 measured by flow cytometry. Data are presented as mean ± SD. (n = 3) III) The relative activity of SPart-P1/HAL and SPart-$P_{6\,h}$/HAL after immobilization at pH 4, 6 and 8 when comparing the conversion of histidine (0.5 mm) into *trans*-urocanic acid within 2 h. Data are presented as mean ± SD. (n = 3). Reproduced with permission from Ref. [163]. Copyright 2023 Wiley.

4.5. Life and health

The application of SI-ATRP in the medical field extends beyond biosensing and medical imaging to drug delivery and antimicrobial coatings. The practical mechanism of drug delivery is also based on responsive materials, where the control of drug release is based on time, temperature, pH, etc [157].

Poly(*N*-vinylcaprolactam) (PNVCL) undergoes a reversible phase transition from hydrophilic to hydrophobic at a critical temperature of ~32 ℃ [158], a property that could be used to regulate drug release, making it a "smart" material for drug delivery applications. PNVCL-coated magnetic nanoparticles could effectively control drug release, particularly for poorly water soluble drugs, due to its pH-responsive and thermoresponsive properties [159]. Asgari et al. [160] prepared chitosan-grafted PNVCL-coated core–shell Fe_3O_4@SiO_2 nanoparticles, which effectively enhanced the solubility, loading capacity and targeted delivery of poorly soluble drugs and improved the therapeutic efficacy and bioavailability of hydrophobic drugs.

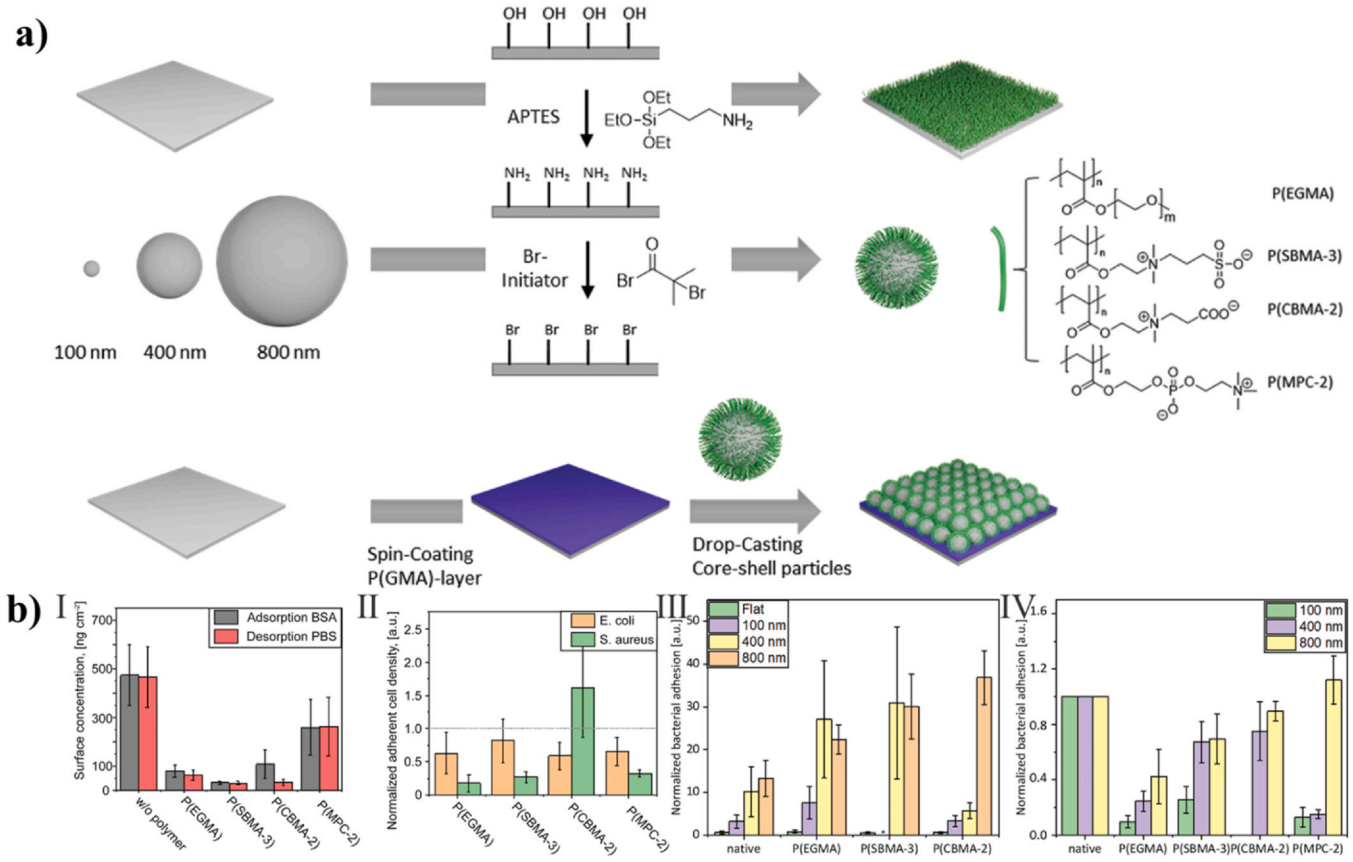

Fig. 17. a) Native flat silicon wafers and spherical SiO_2 particles (100, 400 and 800 nm) were modified with APTES and Br-initiator. Performing SI-ATRP grafting-from polymerization, the surfaces were modified with zwitterionic polymer brushes, namely P(SBMA-3), P(CBMA-2) and P(MPC-2). Finally, the core-shell particles were processed into multilayer particle coatings. b) (I) Adsorbed amount of bovine serum albumin on polymer-modified surfaces, determined by quartz crystal microbalance measurements. The protein solution was adsorbed to the samples for 1 h and subsequently subjected to a desorption regime for 30 min with PBS. (II) Normalized adherent cell densities of *Staphylococcus aureus* (*S. aureus*) and *Escherichia coli* (*E. coli*) on polymer-modified surfaces. Data are normalized by the average adherent cell density on an RCA-cleaned silica substrate. Graphs show the mean ± SD. Data were obtained from at least three independent experiments. Normalized adherent *E. coli* cell density on particle-based surfaces. Data are normalized to (III) the average adherent cell density on an RCA-cleaned silica substrate or to (IV) the non-polymer modified particle-based surface of the respective particle size. Graphs show the mean value ± SD. Data were obtained from at least three independent experiments. Reproduced with permission from Ref. [165]. Copyright 2023 Wiley.

By grafting antimicrobial agent from inorganic nanoparticles, such as gold and silver, the antimicrobial effects can be maximized, and the targeted delivery mechanisms can be employed for specific regions. Cui et al. [161] prepared hemoglobin imprinted poly(ionic liquid)s from the surface of gold nanoparticles *via se*-ATRP, and utilized them as electrochemical sensors. Compared to other hemoglobin sensors based on molecularly imprinted polymers, this biosensor exhibited a wider linear range and lower detection limit, demonstrating promising applications. Han et al. [162] prepared a (2-(methacryloyloxy)ethyl methanesulfonate, MSEA)-based myoglobin (Mb) molecular-imprinted polymers (MIPMSEA) on the surface of a gold electrode decorated with three-dimensional foam graphene (FG) and nanosized gold (nAu). The resulting Au/FG/nAu/MIPMSEA electrode was employed as an electrochemical sensor for detecting Mb. Experimental results suggest that this biosensor offers good selectivity, reproducibility, repeatability and stability. Compared to other methods for detecting Mb, this sensor offered a wider detection range and lower detection limit.

For other responsive materials, Marcelino et al. [163] attached PDEAEMA with hydrophilic and pH-responsive properties to the surface of silica using both “grafting-from” and “grafting-onto” methods (Fig. 16). They then deposited histidine ammonia-lyase (HAL) within the brushes. The "grafting-from" method produces highly dense and uniformly distributed polymer brushes, which creates more surface area and more sites for enzyme deposited, enabling greater protein immobilization and maintaining their catalytic function more effectively. It provided a better choice for achieving high protein immobilization, offering a more suitable environment for HAL deposition after 6 h of polymerization. Gao et al. [164] grafted poly(methacrylic acid (2-(diethylamino)ethyl ester)) (PDEA) onto the surface of Fe_3O_4 coated with SiO_2, using bovine serum albumin as the template for molecular imprinting and dopamine for surface imprinting. The hydrophilicity-hydrophobicity of PDEA can be modulated under alternative stimuli of CO_2 or N_2 gas, enabling the reversible adsorption and release of bovine serum albumin. The resulting CO_2 and magnetic dual-responsive microspheres exhibit advantages such as mild operational conditions, good reversibility, high adsorption capacity and selectivity, demonstrating promising potential for protein separation and enrichment.

Anti-fouling is achieved through controlling the surface hydrophilicity of polymer brushes. Kopsch et al. [165] grafted three types of zwitterionic polymer brushes, poly(sulfobetaine methacrylate), poly (carboxybetaine methacrylate) and poly(2-methacryloyloxyethyl phosphorylcholine), from the surfaces of native flat silicon wafers or silica nanoparticles (Fig. 17). The resulting hybrid materials exhibited suppressed bioadhesion. By adjusting the substrate particle size, the surface morphology and roughness were systematically tuned. The impact of substrate curvature on the surface-specific antibiofouling against Gram-negative Escherichia coli was evaluated. The curvature of the surface significantly affects its antifouling properties by influencing bacterial adhesion. In the study, it was observed that surfaces based on smaller particles (100 nm) exhibited lower bacterial adhesion compared to

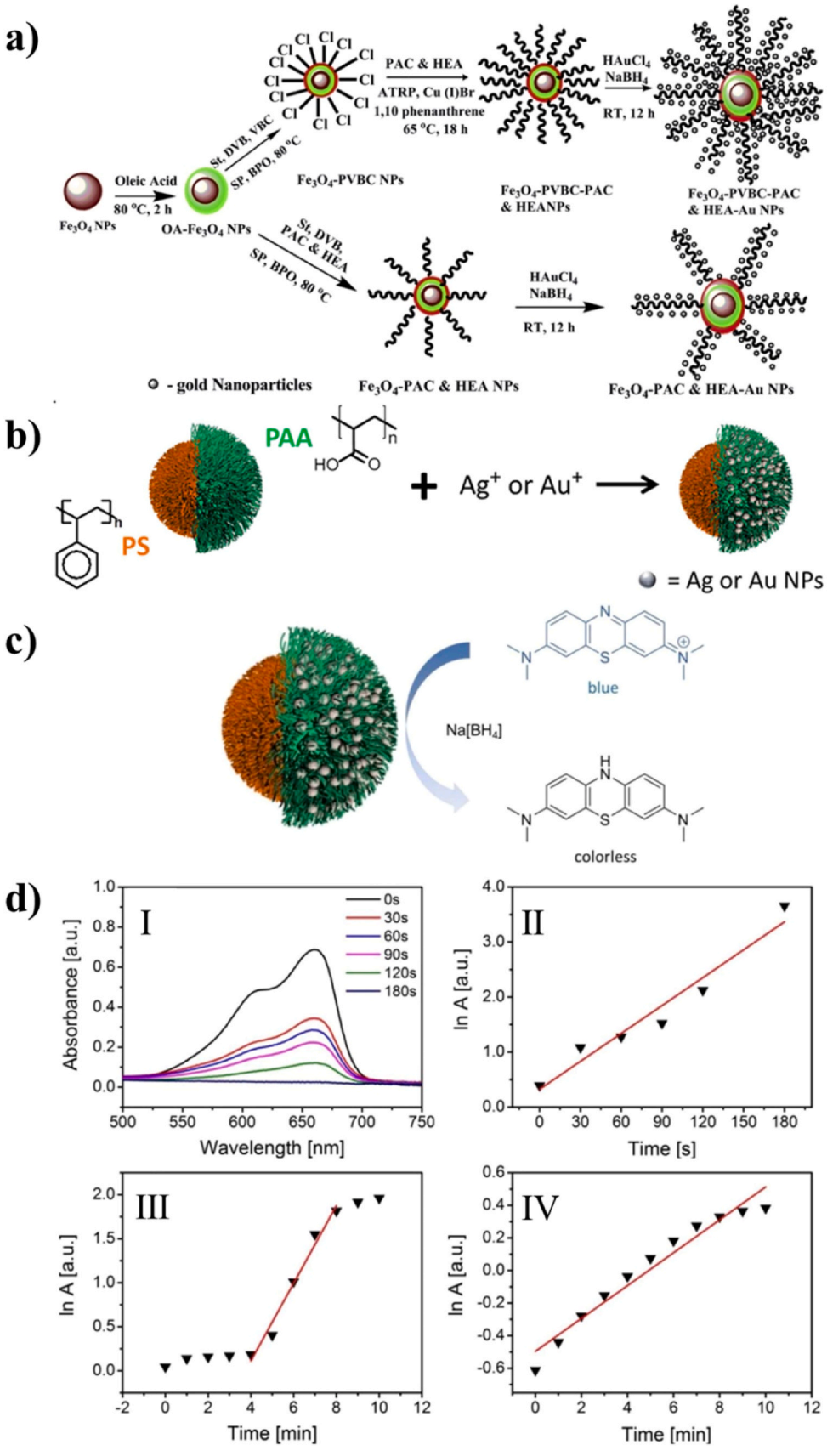

Fig. 18. a) Synthesis of Fe_3O_4-poly(acrylic acid) (PAC) & HEA-Au nanoparticles and Fe_3O_4-PVBC-*g*-PAC & HEA-Au nanoparticles magnetic core-shell based nanocomposite catalysts. b) Scheme of the selective NP immobilization onto PAC/PSt-Janus particles (JP) for catalytic applications. c) Schematic illustration of the catalytic Methylene Blue reduction with sodium borohydride in the presence of Ag NP-modified PAC/PSt-JP. d) (I) UV–vis spectra of the catalytic Methylene Blue reduction; logarithmic plots of the decreasing absorbance over elapsed time for the catalytic reduction of Methylene Blue (II) and Eosin Y (III) in the presence of Ag NP-modified PAC/PSt-JP; (IV) logarithmic plot of the decreasing absorbance over elapsed time for 4-nitrophenol reduction catalyzed by Au nanoparticle-functionalized PAC/PSt-JP.
(a) Reproduced with permission from Ref. [167]. Copyright 2018 Elsevier. (b,c,d) Reproduced with permission from Ref. [168]. Copyright 2015 American Chemical Society.

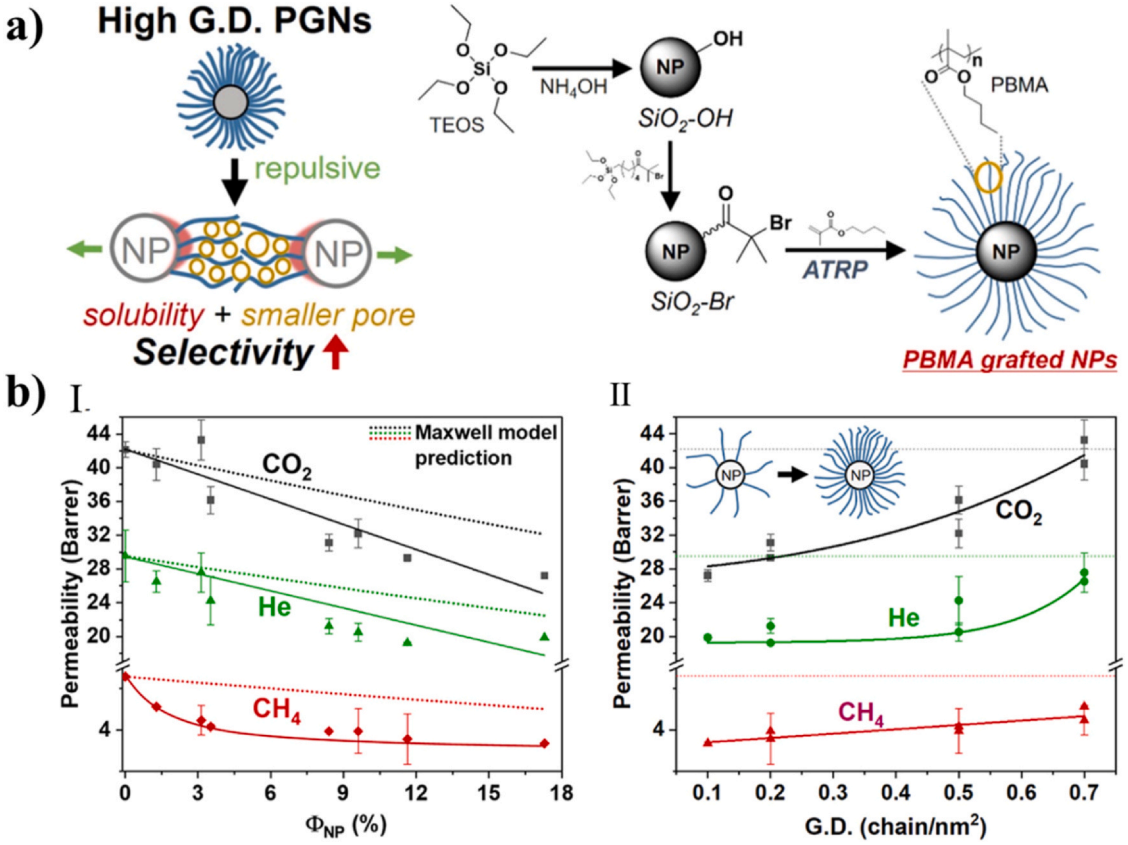

Fig. 19. a) Schematic illustration of PBMA-*g*-NP through ARGET-ATRP and permeability mechanism. b) Permeability of PBMA-*g*-NP membranes plotted versus (I) silica NP volume fraction, Φ_{NP}, with linear (CO_2 and He) and nonlinear (CH_4) fits. Short dotted lines are predictions from the Maxwell model, $P_{eff} = P_m[\frac{P_f + 2P_m - 2\Phi_{NP}(P_m - P_f)}{P_f + 2P_m + \Phi_{NP}(P_m - P_f)}]$, where P_{eff}, P_f and P_m are the permeability of the PGN membranes, the filler (silica NP) and neat PBMA, respectively. For the calculation, we used $P_f = 0$; P_m values are equal to 42.2, 29.5 and 6.6 Barrer for CO_2, He and CH_4, respectively. (II) G.D. with the corresponding exponential growth fits (CO_2 and He) and linear fit (CH_4). Dotted lines are the permeability of CO_2 (gray), He (green) and CH_4 (red) through neat PBMA. Each data point is averaged over at least three experimental points. Reproduced with permission from Ref. [171]. Copyright 2021 American Chemical Society.

surfaces with larger particles (400 nm and 800 nm). This is because surfaces with lower curvature (smaller particles) have a reduced roughness, which minimizes the available surface area for bacteria to adhere. In contrast, surfaces with higher curvature (larger particles) present more complex topographies, increasing roughness and creating more niches that bacteria can colonize. Thus, reducing the curvature radius (using smaller particles) enhances the antifouling performance by limiting bacterial attachment and growth.

4.6. Catalysis

The uniform dispersion of hybrid particles prepared *via* SI-ATRP has profoundly impacted noble metal catalysis. Traditionally, noble metal catalysis is heterogeneous with low selectivity, occurring only at the surface. Traditional noble metal catalysts tend to undergo aggregation similar to other fillers, lowering the effective catalytic surface, undermining the catalytic efficiency [166]. Surface polymer grafting of noble metal nanoparticles allows for increasing catalytic surface through uniform dispersion of catalyst nanoparticles, promoting homogeneous characteristics of the process and thus enhancing catalytic efficiency and selectivity. Ramesh et al. [167] prepared a series of particle brush materials based on magnetic Fe_3O_4 nanoparticle cores through suspension polymerization combined with SI-ATRP (Fig. 18a). Gold nanoparticles were immobilized on the surface of core–shell nanocomposites to obtain recyclable and environmentally friendly metal nano-catalysts with high catalytic activity. Kirillova et al. [168] synthesized a series of large Janus particles on the surface of silica using a combination of Pickering emulsion and “grafting from/grafting to” methods. These particles consisted of a hydrophobic polystyrene polymer shell and a hydrophilic polyacrylic acid polymer shell, with silver and gold nanoparticles embedded in the hydrophilic polymer shell. The hairy Janus particles with immobilized silver or gold nanoparticles effectively catalyzed the reduction of two dyes and a nitro compound by applying a minimal amount of catalyst (Fig. 18b,c).

4.7. Gas separation and barrier

Polymer brush-grafted nanomaterials exhibit significant steric hindrance and adjustable average free volume based on their compositions and architectures [169,170]. Consequently, they hold important research value in the field of gas separation. Through SI-ATRP, polymer chains can be immobilized on the surface of nanoparticles, enabling molecular design of polymer chains in terms of grafting density, molecular weight and grafting units, thereby facilitating the preparation of fine-tuned gas-selective polymer membranes [171,172]. By adjusting graft density and chain length, solute permeabilities can be predictably controlled. Additionally, the grafting process provides mechanical reinforcement to the polymer membranes. Notably, the incorporation of nanoparticles substantially mitigates aging effects typically observed in the systems, presenting a significant improvement over traditional methods that increase free volume using pure polymers [173]. Jeong et al. [171] investigated the influence of structural parameters and material chemistry on the permeability and selectivity of gases (CO_2, Helium and CH_4) in membranes based on poly(glycidyl methacrylate) grafted silica nanoparticles. They found that heterogeneous nanoparticle distribution in particle brushes with low graft density adversely

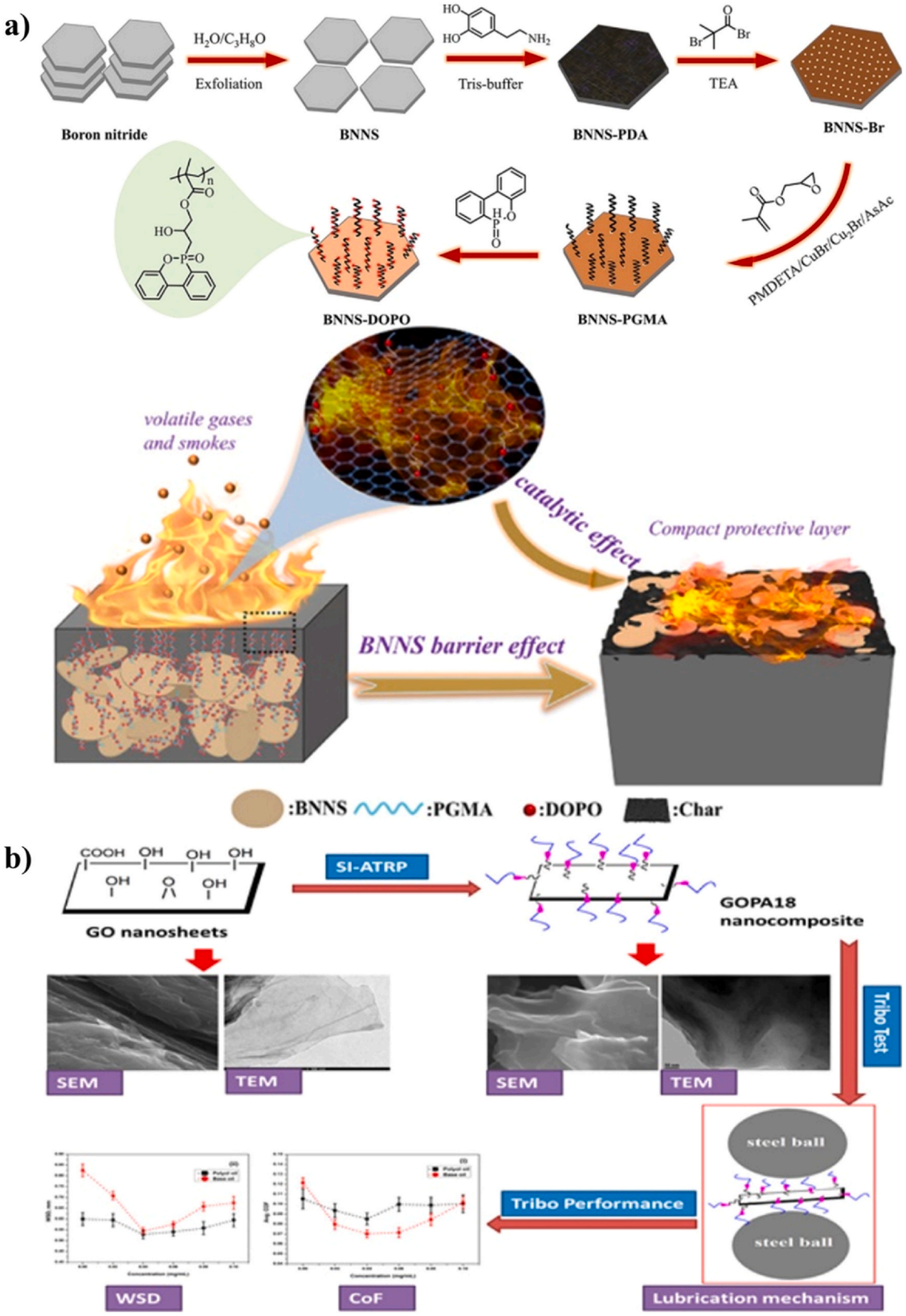

Fig. 20. a) Synthesis method and schematic illustration of the proposed flame-retardant mechanism of the flame-retardant-functionalized boron nitride nanosheet. b) Schematic illustration of synthesis, SEM images, coefficient of friction and wear scar diameter of GOPA18 Nanocomposite by SI-ATRP.
(a) Reproduced with permission from Ref. [177]. Copyright 2022 American Chemical Society. (b) Reproduced with permission from Ref. [178]. Copyright 2016 American Chemical Society.

affects gas diffusion in the membrane. For nanoparticles with high graft density, the homogeneous nanoparticle distribution due to increased polymer coverage on the surface of the particle brushes may increase the free volume of the membrane, contributing to the improvement of the gas permeability (Fig. 19). Thus, this membrane had high selectivity. Wang et al. [174] prepared segmental copolymer particle brushes SiO_2-*g*-PMMA-*b*-poly (ionic liquid)(PIL) based on ionic liquid. Compared to SiO_2-*g*-PIL membranes, the former exhibited a higher Young's modulus while maintaining the membrane's CO_2 permeability and CO_2/N_2 selectivity. Manipulation of the membrane's selective gas transport properties was achieved by controlling the relevant entropy effects through the addition of free chains. The added short free chains were found to uniformly distribute within the polymer layer of the particle brushes, resulting in reduced permeability for all gases without significantly enhancing selectivity. Conversely, free chains with lengths comparable to the grafts were reported to fill the interstitial pockets of the particle brush, preferentially impeding the transport of larger gas molecules, thereby leading to a substantial increase in selectivity [175].

4.8. Other applications

SI-ATRP offers a high degree of freedom in polymer chain structure, enabling polymer-grafted nanoparticles to meet various special application requirements through functionalized polymer chain side groups or terminals [12]. Sulfonation of side epoxy groups can provide cation exchange adsorbents [176]. Introducing flame retarding units through epoxy groups grafted from boron nitride nanoplatelets created nanocomposites with excellent flame retardant performance (Fig. 20a) [177]. Polyacrylates with long aliphatic side chains grafted from graphene oxide were used as high performance lubricant additives (Fig. 20b) [178]. MXenes are a new type of two-dimensional transition-metal carbon/nitride nanomaterials. The introduction of 2D nanosheets into organic coatings improves mechanical characteristics and corrosion resistance [179]. $Ti_3C_2T_x$ is the most studied MXene since it was first discovered in 2011 [180].

Wang et al. [181] employed the SI-ATRP method to functionalize $Ti_3C_2T_x$ with the anticorrosion agent poly(2-mercaptobenzothiazole) (PMBTMA) and the antifouling agent poly(3-sulfopropyl methacrylate potassium) (PSPMA). These functionalized $Ti_3C_2T_x$ particles were then incorporated into a waterborne epoxy resin to fabricate a nanohybrid coating. The PMBTMA component releases the corrosion inhibitor 2-mercaptobenzothiazole in oxidative environments, while the strong hydrophilicity of PSPMA effectively mitigates algal adhesion. The synergistic interaction between $Ti_3C_2T_x$ and PMBTMA further enhances the antibacterial efficacy of 2-mercaptobenzothiazole. The resultant nanohybrid coating demonstrated superior antibacterial performance, with the ability to remove over 55 % of bacteria and up to 71 % of microalgae. Additionally, it exhibited exceptional corrosion resistance, evidenced by an impedance modulus of 3.73×10^7 $\Omega \cdot cm^2$ after 15 days of immersion. Zhang et al. [182] synthesized poly(ionic liquid)-grafted MXene *via* SI-ATRP and incorporated the particle brush into a porous polyurethane 3D network to produce a composite foam using a single-step blending and foaming process. The organic-inorganic hybrid network structure conferred the composite foam with superior mechanical strength, flame resistance and structural integrity.

5. Summary and outlook

Polymer brushes have emerged as a fascinating class of materials with diverse applications. The use of surface-initiated atom transfer radical polymerization (SI-ATRP) enables the fabrication of particle brushes with controllable structure and properties, while advancements in synthesis techniques and the availability of diverse core-shell materials at the molecular level have propelled the development of particle brush materials in terms of structure, functionality and applications. The high specific surface area of core materials and the flexibility of brush materials endow particle brushes with rich interfacial layers, which influence the interactions, assembly behavior and performance of particle brushes. Currently, application-driven functionalized materials are abundant, including stimulus-responsive, “smart” catalytic, energy-dielectric and biomedical materials, expanding the range of material utilization.

Despite the significant advantages of polymer brushes, they still face certain challenges in practical applications. Advanced polymerization techniques and surface modification methods are aimed at overcoming current challenges and further expanding their application scope. Future developments of particle brushes prepared *via* SI-ATRP could consider the following aspects:

1. Interface design and precise synthesis: precise preparation and functionalization of particle brushes *via* rational design of their compositions, architectures and synthetic routes, expanding their applications in catalysis, biomedicine and other fields.
2. Optimization of reaction conditions: further advance SI-ATRP techniques to enhance and broaden their applicability and efficiency in the preparation of particle brushes, and explore less expensive, more scalable and greener processes.
3. Advanced analytical techniques: precise and easier determination of the initiator and polymer brush grafting density is so far challenging [60,183]. This involves determining the efficiency of initiators by a simple, universal and accurate technique to ascertain the number of initiating units/chains per square nanometer of substrate surface. It is hence important to the understanding of the SI-ATRP mechanism on surface and its optimization. In addition, modern analytic tools provide limited information on three-dimensional assembly of particle brushes in bulk and in a matrix. Future development of imaging and scattering/diffraction techniques may provide better insight into these mesoscopic structures.
4. Construction of multifunctional composites: although particle brushes themselves in many cases assemble into quasi-one-component nanocomposites, understanding their interaction with matrices, especially those with functions, has unlimited potential for expanding their applications in electronic devices, sensors and other fields.

CRediT authorship contribution statement

Yingxue Liu: Writing – original draft, Data curation. **Jiadong Wang:** Data curation. **Feichen Cui:** Data curation, Conceptualization. **Yang Han:** Data curation. **Jiajun Yan:** Writing – review & editing, Project administration, Methodology, Conceptualization. **Xuan Qin:** Writing – review & editing, Project administration, Funding acquisition, Conceptualization. **Liqun Zhang:** Supervision, Conceptualization. **Krzysztof Matyjaszewski:** Writing – review & editing, Supervision, Funding acquisition.

Declaration of Competing Interest

The authors declare that they have no known competing financial interests or personal relationships that could have appeared to influence the work reported in this paper.

Acknowledgments

This work was supported by the National Key R&D Program of China (2022YFB3704700). X.Q. gratefully acknowledges financial support from the China Scholarship Council. J.Y. acknowledges financial support from the Science and Technology Commission of Shanghai Municipality (22YF1428200). KM acknowledges support from NSF (DMR 2202747).

References

[1] J.-S. Wang, K. Matyjaszewski, Controlled/"living" radical polymerization. atom transfer radical polymerization in the presence of transition-metal complexes, J. Am. Chem. Soc. 117 (20) (1995) 5614–5615.
[2] K. Matyjaszewski, J. Xia, Atom transfer radical polymerization, Chem. Rev. 101 (9) (2001) 2921–2990.
[3] F. Lorandi, M. Fantin, K. Matyjaszewski, Atom transfer radical polymerization: a mechanistic perspective, J. Am. Chem. Soc. 144 (34) (2022) 15413–15430.
[4] K. Matyjaszewski, Atom Transfer Radical Polymerization (ATRP): current status and future perspectives, Macromolecules 45 (10) (2012) 4015–4039.
[5] K. Matyjaszewski, Advanced materials by atom transfer radical polymerization, Adv. Mater. 30 (23) (2018) 1706441.
[6] J. Yan, M.R. Bockstaller, K. Matyjaszewski, Brush-modified materials: Control of molecular architecture, assembly behavior, properties and applications, Prog. Polym. Sci. 100 (2020) 101180.
[7] K. Matyjaszewski, Current status and outlook for ATRP, Eur. Polym. J. 211 (2024) 113001.
[8] N. Corrigan, K. Jung, G. Moad, C.J. Hawker, K. Matyjaszewski, C. Boyer, Reversible-deactivation radical polymerization (Controlled/living radical polymerization): From discovery to materials design and applications, Prog. Polym. Sci. 111 (2020) 101311.
[9] J. Wang, K. Matyjaszewski, Controlled/"living" radical polymerization. atom transfer radical polymerization in the presence of transition-metal complexes, J. Am. Chem. Soc. 117 (20) (1995) 5614–5615.
[10] J.O. Zoppe, N.C. Ataman, P. Mocny, J. Wang, J. Moraes, H.-A. Klok, Surface-initiated controlled radical polymerization: state-of-the-art, opportunities, and challenges in surface and interface engineering with polymer brushes, Chem. Rev. 117 (3) (2017) 1105–1318.
[11] J.O. Zoppe, N.C. Ataman, P. Mocny, J. Wang, J. Moraes, H.-A. Klok, Correction to surface-initiated controlled radical polymerization: state-of-the-art, opportunities, and challenges in surface and interface engineering with polymer brushes, Chem. Rev. 117 (5) (2017) 4667-4667.
[12] K. Matyjaszewski, N.V. Tsarevsky, Macromolecular engineering by atom transfer radical polymerization, J. Am. Chem. Soc. 136 (18) (2014) 6513–6533.
[13] K. Matyjaszewski, P.J. Miller, N. Shukla, B. Immaraporn, A. Gelman, B.B. Luokala, T.M. Siclovan, G. Kickelbick, T. Vallant, H. Hoffmann, T. Pakula, Polymers at interfaces: using atom transfer radical polymerization in the controlled growth of homopolymers and block copolymers from silicon surfaces in the absence of untethered sacrificial initiator, Macromolecules 32 (26) (1999) 8716–8724.
[14] L. Bombalski, K. Min, H. Dong, C. Tang, K. Matyjaszewski, Preparation of well-defined hybrid materials by ATRP in miniemulsion, Macromolecules 40 (21) (2007) 7429–7432.
[15] R. Yin, P. Chmielarz, I. Zaborniak, Y. Zhao, G. Szczepaniak, Z. Wang, T. Liu, Y. Wang, M. Sun, H. Wu, J. Tarnsangpradit, M.R. Bockstaller, K. Matyjaszewski, Miniemulsion SI-ATRP by interfacial and ion-pair catalysis for the synthesis of nanoparticle brushes, Macromolecules 55 (15) (2022) 6332–6340.
[16] K. Matyjaszewski, Mechanistic and synthetic aspects of atom transfer radical polymerization, J. Macromol. Sci. Part A 34 (10) (1997) 1785–1801.
[17] J. Wang, K. Matyjaszewski, "Living"/controlled radical polymerization. transition-metal-catalyzed atom transfer radical polymerization in the presence of a conventional radical initiator, Macromolecules 28 (22) (1995) 7572–7573.
[18] G. Szczepaniak, L. Fu, H. Jafari, K. Kapil, K. Matyjaszewski, Making ATRP more practical: oxygen tolerance, Acc. Chem. Res. 54 (7) (2021) 1779–1790.
[19] X. Pan, M. Fantin, F. Yuan, K. Matyjaszewski, Externally controlled atom transfer radical polymerization, Chem. Soc. Rev. 47 (14) (2018) 5457–5490.
[20] X. Hu, R. Yin, J. Jeong, K. Matyjaszewski, Robust miniemulsion photoATRP driven by red and near-infrared light, J. Am. Chem. Soc. 146 (19) (2024) 13417–13426.
[21] X. Hu, G. Szczepaniak, A. Lewandowska-Andralojc, J. Jeong, B. Li, H. Murata, R. Yin, A.M. Jazani, S.R. Das, K. Matyjaszewski, Red-light-driven atom transfer radical polymerization for high-throughput polymer synthesis in open air, J. Am. Chem. Soc. 145 (44) (2023) 24315–24327.
[22] G. Szczepaniak, J. Jeong, K. Kapil, S. Dadashi-Silab, S.S. Yerneni, P. Ratajczyk, S. Lathwal, D.J. Schild, S.R. Das, K. Matyjaszewski, Open-air green-light-driven ATRP enabled by dual photoredox/copper catalysis, Chem. Sci. 13 (39) (2022) 11540–11550.
[23] L. Mueller, W. Jakubowski, W. Tang, K. Matyjaszewski, Successful chain extension of polyacrylate and polystyrene macroinitiators with methacrylates in an ARGET and ICAR ATRP, Macromolecules 40 (18) (2007) 6464–6472.
[24] J. Pietrasik, H. Dong, K. Matyjaszewski, Synthesis of high molecular weight poly (styrene-co-acrylonitrile) copolymers with controlled architecture, Macromolecules 39 (19) (2006) 6384–6390.
[25] W. Jakubowski, K. Matyjaszewski, Activators regenerated by electron transfer for atom-transfer radical polymerization of (meth) acrylates and related block copolymers, Angew. Chem. Int. Ed. 45 (27) (2006) 4482–4486.
[26] K. Min, H. Gao, K. Matyjaszewski, Use of ascorbic acid as reducing agent for synthesis of well-defined polymers by ARGET ATRP, Macromolecules 40 (6) (2007) 1789–1791.
[27] K. Matyjaszewski, W. Jakubowski, K. Min, W. Tang, J. Huang, W.A. Braunecker, N.V. Tsarevsky, Diminishing catalyst concentration in atom transfer radical polymerization with reducing agents, Proc. Natl. Acad. Sci. 103 (42) (2006) 15309–15314.
[28] Y. Zhang, Y. Wang, K. Matyjaszewski, ATRP of methyl acrylate with metallic zinc, magnesium, and iron as reducing agents and supplemental activators, Macromolecules 44 (4) (2011) 683–685.
[29] P. Chmielarz, J. Yan, P. Krys, Y. Wang, Z. Wang, M.R. Bockstaller, K. Matyjaszewski, Synthesis of nanoparticle copolymer brushes via surface-initiated se ATRP, Macromolecules 50 (11) (2017) 4151–4159.
[30] A.J. Magenau, N.C. Strandwitz, A. Gennaro, K. Matyjaszewski, Electrochemically mediated atom transfer radical polymerization, Science 332 (6025) (2011) 81–84.
[31] P. Chmielarz, M. Fantin, S. Park, A.A. Isse, A. Gennaro, A.J.D. Magenau, A. Sobkowiak, K. Matyjaszewski, Electrochemically mediated atom transfer radical polymerization (eATRP), Prog. Polym. Sci. 69 (2017) 47–78.
[32] X. Pan, C. Fang, M. Fantin, N. Malhotra, W.Y. So, L.A. Peteanu, A.A. Isse, A. Gennaro, P. Liu, K. Matyjaszewski, Mechanism of photoinduced metal-free atom transfer radical polymerization: experimental and computational studies, J. Am. Chem. Soc. 138 (7) (2016) 2411–2425.
[33] X. Pan, M.A. Tasdelen, J. Laun, T. Junkers, Y. Yagci, K. Matyjaszewski, Photomediated controlled radical polymerization, Prog. Polym. Sci. 62 (2016) 73–125.
[34] M. Cvek, J. Kollar, M. Mrlik, M. Masar, P. Suly, M. Urbanek, J. Mosnacek, Surface-initiated mechano-ATRP as a convenient tool for tuning of bidisperse magnetorheological suspensions toward extreme kinetic stability, Polym. Chem. 12 (35) (2021) 5093–5105.
[35] H. Mohapatra, M. Kleiman, A.P. Esser-Kahn, Mechanically controlled radical polymerization initiated by ultrasound, Nat. Chem. 9 (2) (2017) 135–139.
[36] Z. Wang, X. Pan, J. Yan, S. Dadashi-Silab, G. Xie, J. Zhang, Z. Wang, H. Xia, K. Matyjaszewski, Temporal control in mechanically controlled atom transfer radical polymerization using low ppm of Cu catalyst, ACS Macro Lett. 6 (5) (2017) 546–549.
[37] C. Wang, R. Zhao, W. Fan, L. Li, H. Feng, Z. Li, C. Yan, X. Shao, K. Matyjaszewski, Z. Wang, Tribochemically controlled atom transfer radical polymerization enabled by contact electrification, Angew. Chem. Int. Ed. 62 (37) (2023) e202309440.
[38] Z. Wang, Z. Wang, X. Pan, L. Fu, S. Lathwal, M. Olszewski, J. Yan, A.E. Enciso, Z. Wang, H. Xia, K. Matyjaszewski, Ultrasonication-induced aqueous atom transfer radical polymerization, ACS Macro Lett. 7 (3) (2018) 275–280.
[39] D.A. Corbin, G.M. Miyake, Photoinduced Organocatalyzed Atom Transfer Radical Polymerization (O-ATRP): precision polymer synthesis using organic photoredox catalysis, Chem. Rev. 122 (2) (2022) 1830–1874.
[40] N.J. Treat, H. Sprafke, J.W. Kramer, P.G. Clark, B.E. Barton, J. Read de Alaniz, B.P. Fors, C.J. Hawker, Metal-free atom transfer radical polymerization, J. Am. Chem. Soc. 136 (45) (2014) 16096–16101.
[41] L. Wu, U. Glebe, A. Boeker. Surface-initiated controlled radical polymerizations from silica nanoparticles, gold nanocrystals, and bionanoparticles, Polym. Chem. 6 (29) (2015) 5143–5184.
[42] B. Radhakrishnan, R. Ranjan, W.J. Brittain, Surface initiated polymerizations from silica nanoparticles, Soft Matter 2 (2006) 386–396.
[43] Y. Liu, Z. Wang, Y. Zhao, G. Hou, R. Jiang, M.R. Bockstaller, X. Qin, L. Zhang, K. Matyjaszewski, SiO2-g-polyisoprene particle brush reinforced advanced elastomer nanocomposites prepared via ARGET ATRP, Adv. Funct. Mater. 34 (26) (2024) 2315741.
[44] Y. Zhao, Z. Wang, G. Hou, H. Wu, L. Fu, M.R. Bockstaller, X. Qin, L. Zhang, K. Matyjaszewski, Synthesis of mechanically robust very high molecular weight polyisoprene particle brushes by atom transfer radical polymerization, ACS Macro Lett. 13 (4) (2024) 415–422.
[45] M. Wagner, A. Krieger, F. Gröhn, Gold nanoparticles in disulfide based polymer matrices: size, structure and responsivity, Macromol. Chem. Phys. 225 (4) (2024) 2300342.
[46] Y. Kitayama, T. Takeuchi, Synthesis of CO2/N2-triggered reversible stability-controllable poly(2-(diethylamino)ethyl methacrylate)-grafted-AuNPs by surface-initiated atom transfer radical polymerization, Langmuir 30 (42) (2014) 12684–12689.
[47] L. Cheng, A. Liu, S. Peng, H. Duan, Responsive plasmonic assemblies of amphiphilic nanocrystals at oil – water interfaces, ACS Nano 4 (10) (2010) 6098–6104.
[48] C. Cobo Sánchez, M. Wåhlander, N. Taylor, L. Fogelström, E. Malmström, Novel nanocomposites of poly(lauryl methacrylate)-grafted Al2O3 nanoparticles in LDPE, ACS Appl. Mater. Interfaces 7 (46) (2015) 25669–25678.
[49] F. Arjmand, Z. Mohamadnia, Fabrication of a light-responsive polymer nanocomposite containing spiropyran as a sensor for reversible recognition of metal ions, Polym. Chem. 13 (7) (2022) 937–945.
[50] C. Tuncer, C. Yurdakul, Preparation of metal-containing zwitterionic Fe3O4@SiO2-βPDMA composite systems and catalytic activity studies, ChemistrySelect 9 (11) (2024).
[51] A. Gruszkiewicz, M. Slowikowska, G. Grzes, A. Wojcik, J. Rokita, A. Fiocco, M. Wytrwal-Sarna, M. Marzec, B. Trzebicka, M. Kopec, K. Wolski, S. Zapotoczny, Enhancement of the growth of polymer brushes via ATRP initiated from ions-releasing indium tin oxide substrates, Eur. Polym. J. 112 (2019) 817–821.
[52] B. Zhang, N. Hu, Y. Wang, Z. Wang, Y. Wang, E.S. Kong, Y. Zhang, Poly(glycidyl methacrylates)-grafted zinc oxide nanowire by surface-initiated atom transfer radical polymerization, Nano-Micro Lett. 2 (4) (2010) 285–289.
[53] J. Yan, X. Pan, Z. Wang, Z. Lu, Y. Wang, L. Liu, J. Zhang, C. Ho, M.R. Bockstaller, K. Matyjaszewski, A fatty acid-inspired tetherable initiator for surface-initiated atom transfer radical polymerization, Chem. Mater. 29 (11) (2017) 4963–4969.
[54] K. Ohno, T. Morinaga, K. Koh, Y. Tsujii, T. Fukuda, Synthesis of monodisperse silica particles coated with well-defined, high-density polymer brushes by surface-initiated atom transfer radical polymerization, Macromolecules 38 (6) (2005) 2137–2142.
[55] X. Peng, Y. Chen, F. Li, W. Zhou, Y. Hu, Preparation and optical properties of ZnO@PPEGMA nanoparticles, Appl. Surf. Sci. 255 (16) (2009) 7158–7163.
[56] M. Joafshan, A. Shakeri, S.R. Razavi, H. Salehi, Gas responsive magnetic nanoparticle as novel draw agent for removal of Rhodamine B via forward osmosis: high water flux and easy regeneration, Sep. Purif. Technol. 282 (2022) 119998.
[57] D.Y. Joh, F. McGuire, R. Abedini-Nassab, J.B. Andrews, R.K. Achar, Z. Zimmers, D. Mozhdehi, R. Blair, F. Albarghouthi, W. Oles, J. Richter, C.M. Fontes,

A.M. Hucknall, B.B. Yellen, A.D. Franklin, A. Chilkoti, Poly(oligo(ethylene glycol) methyl ether methacrylate) brushes on high-κ metal oxide dielectric surfaces for bioelectrical environments, ACS Appl. Mater. Interfaces 9 (6) (2017) 5522–5529.
[58] F.M. Albarghouthi, D. Semeniak, I. Khanani, J.L. Doherty, B.N. Smith, M. Salfity, Q. MacFarlane, A. Karappur, S.G. Noyce, N.X. Williams, D.Y. Joh, J.B. Andrews, A. Chilkoti, A.D. Franklin, Addressing signal drift and screening for detection of biomarkers with carbon nanotube transistors, ACS Nano 18 (7) (2024) 5698–5711.
[59] J. Yan, S. Li, F. Cartieri, Z. Wang, T.K. Hitchens, J. Leonardo, S.E. Averick, K. Matyjaszewski, Iron oxide nanoparticles with grafted polymeric analogue of dimethyl sulfoxide as potential magnetic resonance imaging contrast agents, ACS Appl. Mater. Interfaces 10 (26) (2018) 21901–21908.
[60] F. Cui, Y. Sui, Y. Zhang, Z. Xie, J. Yan, Silica etching without HF in particle brushes, ACS Chem. Health Saf. 30 (6) (2023) 392–398.
[61] S.W. Kim, S. Kim, J.B. Tracy, A. Jasanoff, M.G. Bawendi, Phosphine oxide polymer for water-soluble nanoparticles, J. Am. Chem. Soc. 127 (13) (2005) 4556–4557.
[62] W. Cheng, X. Zeng, H. Chen, Z. Li, W. Zeng, L. Mei, Y. Zhao, Versatile polydopamine platforms: synthesis and promising applications for surface modification and advanced nanomedicine, ACS Nano 13 (8) (2019) 8537–8565.
[63] M. Kopeć, J. Spanjers, E. Scavo, D. Ernens, J. Duvigneau, G. Julius Vancso, Surface-initiated ATRP from polydopamine-modified TiO2 nanoparticles, Eur. Polym. J. 106 (2018) 291–296.
[64] J. Yan, M.H. Malakooti, Z. Lu, Z. Wang, N. Kazem, C. Pan, M.R. Bockstaller, C. Majidi, K. Matyjaszewski, Solution processable liquid metal nanodroplets by surface-initiated atom transfer radical polymerization, Nat. Nanotechnol. 14 (7) (2019) 684–690.
[65] H. Kong, C. Gao, D. Yan, Controlled functionalization of multiwalled carbon nanotubes by in situ atom transfer radical polymerization, J. Am. Chem. Soc. 126 (2) (2004) 412–413.
[66] F. Jiang, Y. Zhang, Z. Wang, H. Fang, Y. Ding, H. Xu, Z. Wang, Synthesis and characterization of nanostructured copolymer-grafted multiwalled carbon nanotube composite thermoplastic elastomers toward unique morphology and strongly enhanced mechanical properties, Ind. Eng. Chem. Res. 53 (52) (2014) 20154–20167.
[67] H. Xu, Y. Sang, B. Xu, L. Zhang, L. Zhang, H. Xu, Immobilization of gold nanoparticles on poly(4-vinylpyridine)-grafted carbon nanotubes as heterogeneous catalysts for hydrogenation of 4-nitrophenol, ACS Appl. Nano Mater. 3 (12) (2020) 12169–12177.
[68] C.M. Hui, J. Pietrasik, M. Schmitt, C. Mahoney, J. Choi, M.R. Bockstaller, K. Matyjaszewski, Surface-initiated polymerization as an enabling tool for multifunctional (nano-)engineered hybrid materials, Chem. Mater. 26 (1) (2014) 745–762.
[69] J. Pietrasik, C.M. Hui, W. Chaladaj, H. Dong, J. Choi, J. Jurczak, M.R. Bockstaller, K. Matyjaszewski, Silica-polymethacrylate hybrid particles synthesized using high-pressure atom transfer radical polymerization, Macromol. Rapid Commun. 32 (3) (2011) 295–301.
[70] R.W. Simms, M.F. Cunningham, High molecular weight poly(butyl methacrylate) by reverse atom transfer radical polymerization in miniemulsion initiated by a redox system, Macromolecules 40 (4) (2007) 860–866.
[71] Z. Wang, T. Liu, K.C. Lin, S. Li, J. Yan, M. Olszewski, J. Sobieski, J. Pietrasik, M.R. Bockstaller, K. Matyjaszewski, Synthesis of ultra-high molecular weight SiO2-g-PMMA particle brushes, J. Inorg. Organomet. Polym. Mater. 30 (1) (2020) 174–181.
[72] W.A. Pryor, J.H. Coco, Computer simulation of the polymerization of styrene. The mechanism of thermal initiation and the importance of primary radical termination, Macromolecules 3 (5) (1970) 500–508.
[73] N. Dan, M. Tirrell, Effect of bimodal molecular weight distribution on the polymer brush, Macromolecules 26 (24) (1993) 6467–6473.
[74] Z. Wang, J. Yan, T. Liu, Q. Wei, S. Li, M. Olszewski, J. Wu, J. Sobieski, M. Fantin, M.R. Bockstaller, Control of dispersity and grafting density of particle brushes by variation of ATRP catalyst concentration, ACS Macro Lett. 8 (7) (2019) 859–864.
[75] J. Listak, W. Jakubowski, L. Mueller, A. Plichta, K. Matyjaszewski, M.R. Bockstaller, Effect of symmetry of molecular weight distribution in block copolymers on formation of “metastable” morphologies, Macromolecules 41 (15) (2008) 5919–5927.
[76] Z. Wang, M. Fantin, J. Sobieski, Z. Wang, J. Yan, J. Lee, T. Liu, S. Li, M. Olszewski, M.R. Bockstaller, K. Matyjaszewski, Pushing the limit: synthesis of SiO2-g-PMMA/PS particle brushes via ATRP with very low concentration of functionalized SiO2-Br nanoparticles, Macromolecules 52 (22) (2019) 8713–8723.
[77] X. Jiang, B. Zhao, G. Zhong, N. Jin, J.M. Horton, L. Zhu, R.S. Hafner, T.P. Lodge, Microphase separation of high grafting density asymmetric mixed homopolymer brushes on silica particles, Macromolecules 43 (19) (2010) 8209–8217.
[78] A.A. Brown, N.S. Khan, L. Steinbock, W.T. Huck, Synthesis of oligo (ethylene glycol) methacrylate polymer brushes, Eur. Polym. J. 41 (8) (2005) 1757–1765.
[79] D.M. Jones, A.A. Brown, W.T. Huck, Surface-initiated polymerizations in aqueous media: effect of initiator density, Langmuir 18 (4) (2002) 1265–1269.
[80] Z. Wang, T. Liu, K.C. Lin, S. Li, J. Yan, M. Olszewski, J. Sobieski, J. Pietrasik, M.R. Bockstaller, K. Matyjaszewski, Synthesis of ultra-high molecular weight SiO2-g-PMMA particle brushes, J. Inorg. Organomet. Polym. Mater. 30 (1) (2020) 174–181.
[81] Z. Wang, J. Lee, Z. Wang, Y. Zhao, J. Yan, Y. Lin, S. Li, T. Liu, M. Olszewski, J. Pietrasik, M.R. Bockstaller, K. Matyjaszewski, Tunable assembly of block copolymer tethered particle brushes by surface-initiated atom transfer radical polymerization, ACS Macro Lett. 9 (6) (2020) 806–812.
[82] D.L. Patton, K.A. Page, E.A. Hoff, M.J. Fasolka, K.L. Beers, A robust and high-throughput measurement platform for monomer reactivity ratios from surface-initiated polymerization, Polym. Chem. 3 (5) (2012) 1174–1181.
[83] D.L. Patton, K.A. Page, C. Xu, K.L. Genson, M.J. Fasolka, K.L. Beers, Measurement of reactivity ratios in surface-initiated radical copolymerization, Macromolecules 40 (17) (2007) 6017–6020.
[84] J.-B. Kim, W. Huang, M.L. Bruening, G.L. Baker, Synthesis of triblock copolymer brushes by surface-initiated atom transfer radical polymerization, Macromolecules 35 (14) (2002) 5410–5416.
[85] G. Morgese, L. Trachsel, M. Romio, M. Divandari, S.N. Ramakrishna, E.M. Benetti, Topological polymer chemistry enters surface science: linear versus cyclic polymer brushes, Angew. Chem. 128 (50) (2016) 15812–15817.
[86] R. Rotzoll, P. Vana, Synthesis of poly (methyl acrylate) loops grafted onto silica nanoparticles via reversible addition-fragmentation chain transfer polymerization, J. Polym. Sci. Part A Polym. Chem. 46 (23) (2008) 7656–7666.
[87] P. Mocny, M. Menétrey, H.-A. Klok, Synthesis of loop poly (methyl methacrylate) brushes via chain-end postpolymerization modification, Macromolecules 52 (21) (2019) 8394–8403.
[88] E.M. Benetti, M. Divandari, S.N. Ramakrishna, G. Morgese, W. Yan, L. Trachsel, Loops and cycles at surfaces: the unique properties of topological polymer brushes, Chem. Eur. J. 23 (51) (2017) 12433–12442.
[89] P. Mocny, M. Menetrey, H.-A. Klok, Synthesis of loop poly(methyl methacrylate) brushes via chain-end postpolymerization modification, Macromolecules 52 (21) (2019) 8394–8403.
[90] S. Morsch, W. Schofield, J. Badyal, Tailoring the density of surface-tethered bottlebrushes, Langmuir 27 (23) (2011) 14151–14159.
[91] P. Mocny, H.-A. Klok, Complex polymer topologies and polymer—nanoparticle hybrid films prepared via surface-initiated controlled radical polymerization, Prog. Polym. Sci. 100 (2020) 101185.
[92] C. Xu, S.E. Barnes, T. Wu, D.A. Fischer, D.M. DeLongchamp, J.D. Batteas, K.L. Beers, Solution and surface composition gradients via microfluidic confinement: fabrication of a statistical-copolymer-brush composition gradient, Adv. Mater. 18 (11) (2006) 1427–1430.
[93] M. Fantin, S.N. Ramakrishna, J. Yan, W. Yan, M. Divandari, N.D. Spencer, K. Matyjaszewski, E.M. Benetti, The role of Cu0 in surface-initiated atom transfer radical polymerization: tuning catalyst dissolution for tailoring polymer interfaces, Macromolecules 51 (17) (2018) 6825–6835.
[94] K. Matyjaszewski, M.J. Ziegler, S.V. Arehart, D. Greszta, T. Pakula, Gradient copolymers by atom transfer radical copolymerization, J. Phys. Org. Chem. 13 (12) (2000) 775–786.
[95] Z. Wang, T. Liu, Y. Zhao, J. Lee, Q. Wei, J. Yan, S. Li, M. Olszewski, R. Yin, Y. Zhai, M.R. Bockstaller, K. Matyjaszewski, Synthesis of gradient copolymer grafted particle brushes by ATRP, Macromolecules 52 (24) (2019) 9466–9475.
[96] Y. Zhao, R. Yin, H. Wu, Z. Wang, Y. Zhai, K. Kim, C. Do, K. Matyjaszewski, M.R. Bockstaller, Sequence-enhanced self-healing in “lock-and-key” copolymers, ACS Macro Lett. 12 (4) (2023) 475–480.
[97] R. Yin, Y. Zhao, J. Jeong, J. Tarnsangpradit, T. Liu, S.Y. An, Y. Zhai, X. Hu, M.R. Bockstaller, K. Matyjaszewski, Composition-orientation induced mechanical synergy in nanoparticle brushes with grafted gradient copolymers, Macromolecules 56 (23) (2023) 9626–9635.
[98] Y. Zhao, Z. Wang, C. Yu, H. Wu, M. Olszewski, R. Yin, Y. Zhai, T. Liu, A. Coronado, K. Matyjaszewski, M.R. Bockstaller, Topologically induced heterogeneity in gradient copolymer brush particle materials, Macromolecules 55 (19) (2022) 8846–8856.
[99] Y. Zhao, H. Wu, R. Yin, C. Yu, K. Matyjaszewski, M.R. Bockstaller, Copolymer brush particle hybrid materials with “recall-and-repair” capability, Chem. Mater. 35 (17) (2023) 6990–6997.
[100] N.C. Estillore, R.C. Advincula, Stimuli-responsive binary mixed polymer brushes and free-standing films by LbL-SIP, Langmuir 27 (10) (2011) 5997–6008.
[101] N.D. Brault, H.S. Sundaram, C.-J. Huang, Y. Li, Q. Yu, S. Jiang, Two-layer architecture using atom transfer radical polymerization for enhanced sensing and detection in complex media, Biomacromolecules 13 (12) (2012) 4049–4056.
[102] D. Li, X. Sheng, B. Zhao, Environmentally responsive “hairy” nanoparticles: mixed homopolymer brushes on silica nanoparticles synthesized by living radical polymerization techniques, J. Am. Chem. Soc. 127 (17) (2005) 6248–6256.
[103] J. Yan, T. Kristufek, M. Schmitt, Z. Wang, G. Xie, A. Dang, C.M. Hui, J. Pietrasik, M.R. Bockstaller, K. Matyjaszewski, Matrix-free particle brush system with bimodal molecular weight distribution prepared by SI-ATRP, Macromolecules 48 (22) (2015) 8208–8218.
[104] J. Yom, S.M. Lane, R.A. Vaia, Multi-component hierarchically structured polymer brushes, Soft Matter 8 (48) (2012) 12009–12016.
[105] F. Cui, Y. Zhang, Y. Sui, H. Chen, B.A. Helms, J. Yan, Rewritable surface-grafted polymer brushes with dynamic covalent linkages, Angew. Chem. Int. Ed. n/a (n/a) (2024) e202410862.
[106] L.H. Baekeland, The synthesis, constitution, and uses of bakelite, J. Ind. Eng. Chem. 1 (3) (1909) 149–161.
[107] A. Charlesby, J. Morris, P. Montague, Mechanisms of reinforcement of silicone rubbers crosslinked by radiation, J. Polym. Sci. Part C Polym. Symp. 16 (8) (1967) 4505–4513.
[108] J. Choi, C.M. Hui, J. Pietrasik, H. Dong, K. Matyjaszewski, M.R. Bockstaller, Toughening fragile matter: mechanical properties of particle solids assembled from polymer-grafted hybrid particles synthesized by ATRP, Soft Matter 8 (15) (2012) 4072–4082.
[109] J.C. Conrad, M.L. Robertson, Shaping the structure and response of surface-grafted polymer brushes via the molecular weight distribution, JACS Au 3 (2) (2023) 333–343.
[110] H.S. Wang, A. Khan, Y. Choe, J. Huh, J. Bang, Architectural effects of organic nanoparticles on block copolymer orientation, Macromolecules 50 (13) (2017) 5025–5032.

[111] W. Wu, M. Singh, A. Masud, X. Wang, A. Nallapaneni, Z. Xiao, Y. Zhai, Z. Wang, T. Terlier, M. Bleuel, G. Yuan, S.K. Satija, J.F. Douglas, K. Matyjaszewski, M.R. Bockstaller, A. Karim, Control of phase morphology of binary polymer grafted nanoparticle blend films via direct immersion annealing, ACS Nano 15 (7) (2021) 12042–12056.
[112] Y. Zhai, J. Han, Y. Zhao, K. Matyjaszewski, M.R. Bockstaller, Processable sub-5 nanometer organosilica hybrid particles for dye stabilization, ACS Appl. Polym. Mater. 3 (7) (2021) 3631–3635.
[113] A. Ma, J. Zhang, N. Wang, L. Bai, H. Chen, W. Wang, H. Yang, L. Yang, Y. Niu, D. Wei, Surface-initiated metal-free photoinduced ATRP of 4-vinylpyridine from SiO2 via visible light photocatalysis for self-healing hydrogels, Ind. Eng. Chem. Res. 57 (51) (2018) 17417–17429.
[114] M. Schmitt, J. Choi, C.M. Hui, B. Chen, E. Korkmaz, J. Yan, S. Margel, O.B. Ozdoganlar, K. Matyjaszewski, M.R. Bockstaller, Processing fragile matter: effect of polymer graft modification on the mechanical properties and processibility of (nano-) particulate solids, Soft Matter 12 (15) (2016) 3527–3537.
[115] J. Choi, H. Dong, K. Matyjaszewski, M.R. Bockstaller, Flexible particle array structures by controlling polymer graft architecture, J. Am. Chem. Soc. 132 (36) (2010) 12537–12539.
[116] J.M. Kubiak, R.J. Macfarlane, Forming covalent crosslinks between polymer-grafted nanoparticles as a route to highly filled and mechanically robust nanocomposites, Adv. Funct. Mater. 29 (44) (2019) 1905168.
[117] S.K. Kumar, N. Jouault, B. Benicewicz, T. Neely, Nanocomposites with polymer grafted nanoparticles, Macromolecules 46 (9) (2013) 3199–3214.
[118] M. Bonnevide, A.M. Jimenez, D. Dhara, T.N.T. Phan, N. Malicki, Z.M. Abbas, B. Benicewicz, S.K. Kumar, M. Couty, D. Gigmes, J. Jestin, Morphologies of polyisoprene-grafted silica nanoparticles in model elastomers, Macromolecules 52 (20) (2019) 7638–7645.
[119] Y. Li, P. Tao, A. Viswanath, B.C. Benicewicz, L.S. Schadler, Bimodal surface ligand engineering: the key to tunable nanocomposites, Langmuir 29 (4) (2013) 1211–1220.
[120] S. Bi, X. Wei, N. Li, Z. Lei, In-situ formation of Fe3O4 nanoparticles within the thermosensitive hairy hybrid particles, Mater. Lett. 62 (17) (2008) 2963–2966.
[121] B.T. Cheesman, J.D. Willott, G.B. Webber, S. Edmondson, E.J. Wanless, pH-responsive brush-modified silica hybrids synthesized by surface-initiated ARGET ATRP, ACS Macro Lett. 1 (10) (2012) 1161–1165.
[122] Y. Eygeris, N. Ulery, I. Zharov, pH-responsive membranes from self-assembly of poly(2-(dimethylamino)ethyl methacrylate) brush silica nanoparticles, Langmuir 39 (44) (2023) 15792–15798.
[123] S. Kim, H.D.D. Sikes, Radical polymerization reactions for amplified biodetection signals, Polym. Chem. 11 (8) (2020) 1424–1444.
[124] F.D. Jochum, P. Theato, Temperature- and light-responsive smart polymer materials, Chem. Soc. Rev. 42 (17) (2013) 7468–7483.
[125] Z. Cao, G. Wang, Multi-stimuli-responsive polymer materials: particles, films, and bulk gels, Chem. Rec. 16 (3) (2016) 1398–1435.
[126] Z. Abousalman-Rezvani, H. Roghani-Mamaqani, H. Riazi, O. Abousalman-Rezvani, Water treatment using stimuli-responsive polymers, Polym. Chem. 13 (42) (2022) 5940–5964.
[127] S. Chakraborty, S.W. Bishnoi, V.H. Pérez-Luna, Gold nanoparticles with poly(N-isopropylacrylamide) formed via surface initiated atom transfer free radical polymerization exhibit unusually slow aggregation kinetics, J. Phys. Chem. C 114 (13) (2010) 5947–5955.
[128] B. Zhang, R. Wang, Poly(ionic liquid) grafted MXene via Si-ATRP and its polyurethane composite foam: mechanical, flame retardant and sensing properties, J. Macromol. Sci., Part B, 1–21. ⟨10.1080/00222348.2023.22908662023⟩.
[129] B. Jiang, Y. Zhang, X. Huang, T. Kang, S.J. Severtson, W.-J. Wang, P. Liu, Tailoring CO2-responsive polymers and nanohybrids for green chemistry and processes, Ind. Eng. Chem. Res. 58 (33) (2019) 15088–15108.
[130] A.K. Gupta, M. Gupta, Synthesis and surface engineering of iron oxide nanoparticles for biomedical applications, Biomaterials 26 (18) (2005) 3995–4021.
[131] S. Iwasaki, H. Kawasaki, Y. Iwasaki, Label-free specific detection and collection of C-reactive protein using zwitterionic phosphorylcholine-polymer-protected magnetic nanoparticles, Langmuir 35 (5) (2019) 1749–1755.
[132] G. Liu, M. Cai, X. Wang, F. Zhou, W. Liu, Core–shell–corona-structured polyelectrolyte brushes-grafting magnetic nanoparticles for water harvesting, ACS Appl. Mater. Interfaces 6 (14) (2014) 11625–11632.
[133] H. Sharifi Dehsari, K. Asadi, Ultrasound-mediated atom transfer radical polymerization for polymer-grafted magnetic nanoparticles with controlled packing density, ACS Appl. Polym. Mater. 6 (5) (2024) 2547–2557.
[134] S. Moradi, R. Najjar, H. Hamishehkar, A. Lotfi, Triple-responsive drug nanocarrier: magnetic core-shell nanoparticles of Fe3O4@poly(N-isopropylacrylamide)-grafted-chitosan, synthesis and in vitro cytotoxicity evaluation against human lung and breast cancer cells, J. Drug Deliv. Sci. Technol. 72 (2022) 103426.
[135] B. Heidari, P. Zarshenas, R. Sedghi, M.R. Nabid, R.S. Varma, Highly selective and sensitive recognition of multi-ions in aqueous solution based on polymer-grafted nanoparticle as visual colorimetric sensor, Sci. Rep. 14 (1) (2024) 213.
[136] E. Diepenbroek, M.B. Pérez, S. de Beer, PNIPAM brushes in colloidal photonic crystals enable ex situ ethanol vapor sensing, ACS Appl. Polym. Mater. 6 (1) (2024) 870–878.
[137] J. Yan, J. Pietrasik, A. Wypych-Puszkarz, M. Ciekanska, K. Matyjaszewski, Synthesis of High κ Nanoparticles by Controlled Radical Polymerization, in Solution-Processable Components for Organic Electronic Devices, (Eds: J. Ulanski, B. Luszczynska, K. Matyjaszewski), 2019, Ch. 3, 181-226.
[138] L. Xie, X. Huang, C. Wu, P. Jiang, Core-shell structured poly(methyl methacrylate)/BaTiO3 nanocomposites prepared by in situ atom transfer radical polymerization: a route to high dielectric constant materials with the inherent low loss of the base polymer, J. Mater. Chem. 21 (16) (2011) 5897–5906.
[139] L. Li, W. Hu, L. Chi, H. Fuchs, Polymer brush and inorganic oxide hybrid nanodielectrics for high performance organic transistors, J. Phys. Chem. B 114 (16) (2010) 5315–5319.
[140] C.A. Grabowski, H. Koerner, J.S. Meth, A. Dang, C.M. Hui, K. Matyjaszewski, M.R. Bockstaller, M.F. Durstock, R.A. Vaia, Performance of dielectric nanocomposites: matrix-free, hairy nanoparticle assemblies and amorphous polymer–nanoparticle blends, ACS Appl. Mater. Interfaces 6 (23) (2014) 21500–21509.
[141] E. Krysiak, A. Wypych-Puszkarz, K. Krysiak, G. Nowaczyk, M. Makrocka-Rydzyk, S. Jurga, J. Ulanski, Core–shell system based on titanium dioxide with elevated value of dielectric permittivity: synthesis and characterization, Synth. Met. 209 (2015) 150–157.
[142] L. Xie, X. Huang, Y. Huang, K. Yang, P. Jiang, Core@double-shell structured BaTiO3–polymer nanocomposites with high dielectric constant and low dielectric loss for energy storage application, J. Phys. Chem. C 117 (44) (2013) 22525–22537.
[143] M. Fantin, A.A. Isse, Improvement of electrode performance by grafting polymers via atom transfer radical polymerization (ATRP): principles and applications, Curr. Opin. Electrochem. 40 (2023) 101313.
[144] Q. Hu, S. Gan, Y. Bao, Y. Zhang, D. Han, L. Niu, Electrochemically controlled ATRP for cleavage-based electrochemical detection of the prostate-specific antigen at femtomolar level concentrations, Anal. Chem. 92 (24) (2020) 15982–15988.
[145] J. Chang, H. Li, L. Yang, H. Liu, Surface-hydrophilic-modified carbon aerogels via surface-initiated electrochemically mediated atom transfer radical polymerization for high-performance supercapacitors, J. Mater. Sci. Mater. Electron. 31 (23) (2020) 21379–21388.
[146] K.H. Khan, Y. Golitsyn, D. Reichert, J. Kressler, H. Hussain, Graphene oxide-grafted hybrid diblock copolymer brush (GO-graft-PEG6k-block-P(MA-POSS)) as nanofillers for enhanced lithium ion conductivity of peo-based nanocomposite solid polymer electrolytes, J. Phys. Chem. B 127 (9) (2023) 2066–2082.
[147] S. Li, T. Liu, J. Yan, J. Flum, H. Wang, F. Lorandi, Z. Wang, L. Fu, L. Hu, Y. Zhao, R. Yuan, M. Sun, J.F. Whitacre, K. Matyjaszewski, Grafting polymer from oxygen-vacancy-rich nanoparticles to enable protective layers for stable lithium metal anode, Nano Energy 76 (2020) 105046.
[148] B.V. Tawade, M. Singh, I.E. Apata, J. Veerasamy, N. Pradhan, A. Karim, J.F. Douglas, D. Raghavan, Polymer-grafted nanoparticles with variable grafting densities for high energy density polymeric nanocomposite dielectric capacitors, JACS Au 3 (5) (2023) 1365–1375.
[149] G.J. Desroches, C.J. Thrasher, N.S. Diaco, I.O. Raji, D. Konkolewicz, A.J. Hart, R.J. Macfarlane, Multivalent polymer-grafted nanoparticles as reinforcing fillers for 3D printable self-healing elastomers, ACS Mater. Lett., 4175-4182. ⟨doi:10.1021/acsmaterialslett.4c012912024⟩.
[150] A. Small, S. Hong, D. Pine, Scattering properties of core-shell particles in plastic matrices, J. Polym. Sci. Part B Polym. Phys. 43 (24) (2005) 3534–3548.
[151] A. Dang, S. Ojha, C.M. Hui, C. Mahoney, K. Matyjaszewski, M.R. Bockstaller, High-transparency polymer nanocomposites enabled by polymer-graft modification of particle fillers, Langmuir 30 (48) (2014) 14434–14442.
[152] P. Chylek, Absorption and scattering of light by small particles, Appl. Opt. 25 (18) (1986) 3166.
[153] L. Bombalski, H. Dong, J. Listak, K. Matyjaszewsk, M.R. Bockstaller, Null-scattering hybrid particles using controlled radical polymerization, Adv. Mater. 19 (24) (2007) 4486–4490.
[154] N. Gao, X. Fang, Synthesis and development of graphene–inorganic semiconductor nanocomposites, Chem. Rev. 115 (16) (2015) 8294–8343.
[155] I. Tokareva, S. Minko, J.H. Fendler, E. Hutter, Nanosensors based on responsive polymer brushes and gold nanoparticle enhanced transmission surface plasmon resonance spectroscopy, J. Am. Chem. Soc. 126 (49) (2004) 15950–15951.
[156] I. Tokarev, I. Tokareva, S. Minko, Optical nanosensor platform operating in near-physiological pH range via polymer-brush-mediated plasmon coupling, ACS Appl. Mater. Interfaces 3 (2) (2011) 143–146.
[157] K.M. El-Say, H.S. El-Sawy, Polymeric nanoparticles: promising platform for drug delivery, Int. J. Pharm. 528 (1) (2017) 675–691.
[158] M.J. Khodabakhshi, H. Ahmad Panahi, E. Konoz, A. Feizbakhsh, S. Kimiagar, NIR-triggered drug delivery system based on Fe3O4-MoS2 core-shell grafted poly(N-vinylcaprolactam): isotherm and kinetics studies, Polym. Plast. Technol. Mater. 60 (11) (2021) 1247–1260.
[159] S. Banihashem, M.N. Nezhati, H.A. Panahia, Synthesis of chitosan-grafted-poly(N-vinylcaprolactam) coated on the thiolated gold nanoparticles surface for controlled release of cisplatin, Carbohydr. Polym. 227 (2020) 115333.
[160] S. Asgari, B. Farasati Far, G. Charmi, P.H. Maghsoudi, S. Keihankhadiv, M. Seyedhamzeh, A.K. Kaushik, Chitosan-grafted-poly(n-vinylcaprolactam)-decorated Fe3O4@SiO2 core–shell nanoformulation as an efficient drug delivery system for poorly soluble drugs, ACS Appl. Bio Mater. 6 (12) (2023) 5809–5827.
[161] A. Cui, Z. Yang, X. Feng, H. Zhao, P. Meng, Y. Xie, L. Miao, Y. Sun, Preparation and properties of hemoglobin (Hb)-imprinted poly (ionic liquid)s via seATRP in only 5 μL Volumes, J. Polym. Res. 29 (9) (2022) 384.
[162] Z. Han, Y. Zhou, Y. Yang, Y. Sun, Y. Wang, Y. Wang, Y. Sun, Preparation of myoglobin-imprinted polymer with a new sulphoxide monomer on the surface of foam-graphene/nano Au via eATRP, Bull. Mater. Sci. 45 (2) (2022) 58.
[163] T. Marcelino, M.A.R. Docampo, X. Qian, C. Ade, E. Brodszkij, M. Ceccato, M. Foss, M. Dulchavsky, J.C.A. Bardwell, B. Städler, Surfaces coated with polymer brushes work as carriers for histidine ammonia lyase, Macromol. Biosci. 23 (8) (2023) 2200528.
[164] J. Gao, X. Yang, Z. Chen, L. Qian, Q. Meng, Z. Li, H. Zhou, H. Liu, L. Ning, CO2 and magnetic dual-responsive microspheres that reversibly and selectively capture target proteins under mild conditions, ACS Appl. Polym. Mater. 5 (2) (2023) 1135–1144.

[165] F. Kopsch, A. Drechsler, M. Priebs, A. Caspari, A. Müller, S. Lentz, J. Friedrichs, A. Synytska, Zwitterionic polymer brushes and core-shell particles based thereon for control of biofouling, Macromol. Chem. Phys. 224 (9) (2023) 2200454.
[166] J.D. Aiken, R.G. Finke, A review of modern transition-metal nanoclusters: their synthesis, characterization, and applications in catalysis, J. Mol. Catal. A Chem. 145 (1) (1999) 1–44.
[167] A. Ramesh, P. Tamizhdurai, S. Gopinath, K. Sureshkumar, E. Murugan, K. Shanthi, Facile synthesis of core-shell nanocomposites Au catalysts towards abatement of environmental pollutant Rhodamine B, Heliyon 5 (1) (2019) e01005.
[168] A. Kirillova, C. Schliebe, G. Stoychev, A. Jakob, H. Lang, A. Synytska, Hybrid hairy janus particles decorated with metallic nanoparticles for catalytic applications, ACS Appl. Mater. Interfaces 7 (38) (2015) 21218–21225.
[169] Y. Yampolskii, Polymeric gas separation membranes, Macromolecules 45 (8) (2012) 3298–3311.
[170] P.M. Budd, K.J. Msayib, C.E. Tattershall, B.S. Ghanem, K.J. Reynolds, N.B. McKeown, D. Fritsch, Gas separation membranes from polymers of intrinsic microporosity, J. Membr. Sci. 251 (1) (2005) 263–269.
[171] S.P. Jeong, R. Kumar, A.-C. Genix, I. Popov, C. Li, S.M. Mahurin, X. Hu, W. Bras, I. Popovs, A.P. Sokolov, V. Bocharova, Improving gas selectivity in membranes using polymer-grafted silica nanoparticles, ACS Appl. Nano Mater. 4 (6) (2021) 5895–5903.
[172] J.D. Moon, B.D. Freeman, C.J. Hawker, R.A. Segalman, Can self-assembly address the permeability/selectivity trade-offs in polymer membranes? Macromolecules 53 (14) (2020) 5649–5654.
[173] C.R. Bilchak, E. Buenning, M. Asai, K. Zhang, C.J. Duming, S.K. Kumar, Y. Huang, B.C. Benicewicz, D.W. Gidley, S. Cheng, A.P. Sokolov, M. Minelli, F. Doghieri, Polymer-grafted nanoparticle membranes with controllable free volume, Macromolecules 50 (18) (2017) 7111–7120.
[174] Z. Wang, Y. Wang, J. Chen, M. Arnould, I. Popovs, S.M. Mahurin, H. Chen, T. Wang, S. Dai, Synthesis of poly(ionic liquid)s-block-poly(methyl methacrylate) copolymer-grafted silica particle brushes with enhanced CO2 permeability and mechanical performance, Langmuir 37 (36) (2021) 10875–10881.
[175] C.R. Bilchak, M. Jhalaria, Y. Huang, Z. Abbas, J. Midya, F.M. Benedetti, D. Parisi, W. Egger, M. Dickmann, M. Minelli, F. Doghieri, A. Nikoubashman, C.J. Durning, D. Vlassopoulos, J. Jestin, Z.P. Smith, B.C. Benicewicz, M. Rubinstein, L. Leibler, S.K. Kumar, Tuning selectivities in gas separation membranes based on polymer-grafted nanoparticles, ACS Nano 14 (12) (2020) 17174–17183.
[176] Z. Mohamadnia, P. Tari, S. Amani, Preparation of smart brush-type cation-exchange adsorbents grafted nanosurface via SI-ATRP for dye removal, Colloids Surf. A Physicochem. Eng. Asp. 624 (2021) 126829.
[177] L. Yang, J. Guo, L. Zhang, C. Li, Significant improvement in the flame retardancy and thermal conductivity of the epoxy resin via constructing a branched flame retardant based on SI-ATRP initiated by dopamine-modified boron nitride, Ind. Eng. Chem. Res. 61 (23) (2022) 8031–8042.
[178] A. Kumar, B. Behera, G.D. Thakre, S.S. Ray, Covalently grafted graphene oxide/poly(cn-acrylate) nanocomposites by surface-initiated ATRP: an efficient anti-friction, antiwear, and pour-point-depressant lubricating additive in oil media, Ind. Eng. Chem. Res. 55 (31) (2016) 8491–8500.
[179] X. Li, S. Zhou, Epoxy-functionalized Ti3C2 nanosheet for epoxy coatings with prominent anticorrosion performance, Prog. Org. Coat. 162 (2022) 106559.
[180] P. Yang, X. Guo, J. Zhang, C. Chen, Y. Gan, W. Xie, Y. Du, Z. Wu, Picomolar thrombin detection by orchestration of triple signal amplification strategy with hierarchically porous Ti3C2Tx MXene electrode material-catalytic hairpin assembly reaction-metallic nanoprobes, Biosens. Bioelectron. 208 (2022) 114228.
[181] P. Wang, B. He, Y. Du, B. Wang, J. Gao, S. Liu, Q. Ye, F. Zhou, Functionalized Ti3C2Tx-based nanocomposite coatings for anticorrosion and antifouling applications, Chem. Eng. J. 448 (2022) 137668.
[182] B. Zhang, R. Wang, Poly(ionic liquid) grafted MXene via Si-ATRP and its polyurethane composite foam: mechanical, flame retardant and sensing properties, J. Macromol. Sci. Part B 63 (10) (2024) 909–929.
[183] L. Michalek, L. Barner, C. Barner-Kowollik, Polymer on top: current limits and future perspectives of quantitatively evaluating surface grafting, Adv. Mater. 30 (21) (2018) 1706321.